Aeroelastic Effect of Corrugation for an Insect-Sized Flapping Wing

Takeshi Minoda[1]
Kyushu University, Fukuoka 8190395, Japan

Hiroto Nagai[2]
Nagasaki University, Nagasaki 8528521, Japan

and
Shigeki Yashiro[3] and Nobuhide Uda[4]
Kyushu University, Fukuoka 8190395, Japan

The fundamental aeroelastic effect of the corrugation of an insect-sized simple flapping wing is numerically investigated. A baseline model for a corrugated flapping wing is constructed such that the balance among the aerodynamic, elastic, and inertial forces acting on the wing matches that acting on insect wings in accordance with the measured material properties of insect wings. The thickness of the corrugated airfoil and the amplitude of corrugation are systematically varied around the baseline to modulate both the natural frequencies and mode shapes. Unsteady aeroelastic simulation based on three-dimensional Naiver–Stokes equations is conducted for the corrugated flapping wings. The numerical simulation is validated by measuring the natural frequency and mean lift of corrugated flapping wings. The results indicate that the corrugation of insect flapping wings is aeroelastically effective in providing both an appropriate passive deformation and a light-weight wing. To maximize the hovering efficiency, the optimal amplitude of corrugation is 1.7 to 2.6% of the chord length, the wing mass ratio is 0.7 to 1.5, and the natural frequency is 2.1 to 2.6 times as large as the input flapping frequency. These optimal design parameters are close to (but slightly smaller than) those of insect wings.

Nomenclature

a_w	=	amplitude of corrugation
c	=	chord length of wing
f_{in}	=	input flapping frequency
f_k	=	kth natural frequency of wing
f_1^*	=	first natural frequency ratio to input flapping frequency
h	=	thickness of wing plate
L	=	lift
m_w	=	wing mass
n_w	=	wave number of corrugation
P^+	=	positive total power
P_i^+	=	positive inertial power
R	=	semispan length of wing
r_{ref}	=	radius of reference span station of wing
z_w	=	corrugation shape
λ	=	wavelength of corrugation

[1] PhD Student, Department of Aeronautics and Astronautics.

[2] Associate Professor, Graduate School of Engineering; nagai.hiroto@nagasaki-u.ac.jp. Senior Member AIAA.

[3] Professor, Department of Aeronautics and Astronautics.

[4] Emeritus Professor, Department of Aeronautics and Astronautics.

η	=	hovering efficiency
θ	=	feathering angle
ξ_k	=	kth modal coordinate
ρ	=	density
ϕ	=	flapping angle
Φ_k	=	kth mode shape of wing
$\psi_{F/F}$	=	phase lead of feathering motion relative to flapping motion
$\psi_{I/O}$	=	phase lag of the first-mode oscillation relative to input flapping oscillation

Subscripts

a	=	air or aerodynamics
def	=	deformation
in	=	input parameter
out	=	output response
w	=	wing structure

Superscripts

–	=	time-averaged value
^	=	amplitude of oscillation
*	=	nondimensional

I. Introduction

FLAPPING-WING-TYPE micro air vehicles (FWMAVs), which mimic the superior flapping flight of birds and insects, have attracted attention for application as a small-sized, human-friendly drone compared with the conventional rotary drones. Although some FWMAVs have attained successful autonomous flight [1–5], there is still a large gap in flight performance between birds and insects and FWMAVs [6]. This fact implies that there still remain unutilized technologies of the flapping flight of birds and insects which can be applied to FWMAVs. Many previous experimental and numerical studies [7–16] have clarified the distinguishing aerodynamics for flapping wings, such as delayed stall, rotational circulation, and wake capture. Extremely light-weight wings of insects are subjected to aeroelastic deformation during a flapping cycle [17,18]. In addition, recent FWMAVs positively utilize passive aeroelastic deformation to achieve complicated wing kinematics with a simple mechanical actuation system [1–5]. Aeroelastic effects of flapping wings have also been investigated in many previous studies. Young et al. [19] and Du and Sun [20] studied the effects of wing deformation on aerodynamics of a flapping wing by actively providing the prescribed deformation based on the measured data of locust and hoverfly wings, respectively. These studies reported that the deformation of the flapping wings enhances lift and improves the aerodynamic efficiency due to the generation of preferable cambered airfoil and spanwise torsion. The effects of aeroelastically passive deformation of flapping wings have been also investigated in numerical [21–27] and experimental studies [28–32]. Some studies considered realistic wing structures of insects or FWMAVs, such as vein arrangement and structural anisotropy [23,25,29,30] and thickness distribution [23,26] and revealed that beneficial wing deformations to improve the aerodynamic characteristics are passively produced by appropriate structural designs. However, the aeroelastic effects of flapping wings have not been sufficiently clarified yet, and it is still unknown what an optimal wing structure for flapping flight is. Therefore, the designs of flapping wings for FWMAVs still depend on trial-and-error experimental methods [1–5].

These previous studies on aeroelastic flapping wings employed a flat plate wing; however, many insects have cambered and corrugated wings instead of flat wings [33–36]. The aerodynamic effects of corrugated wings have been investigated mainly for fixed wings of dragonflies in gliding flight, which are usually used at a lower angle of attack than a flapping wing. Previous studies indicate that corrugated airfoils as a fixed wing are effective for lift enhancement and drag reduction [37,38], stall characteristics [39], and flight dynamic stability [40] due to the trapped vortices inside the valleys of corrugation. For a

corrugated flapping wing, Meng et al. [41] and Meng and Sun [42] numerically investigated the aerodynamic effects of corrugated airfoils of a flapping wing in hovering and forward flight, respectively. Their results indicate that the difference in the aerodynamic characteristics is slight between flat and corrugated flapping wings. Du and Sun [43] and Au et al. [44] provided the corrugated flapping wing with the prescribed deformation in accordance with the measured data of hoverflies and FWMAVs, respectively, and numerically investigated the aerodynamic effects of wing deformation with corrugated airfoils. These results also indicate that the aerodynamic effects of a corrugated flapping wing are small even when the prescribed deformation is provided. Consequently, these previous studies concluded that corrugated airfoils of a flapping wing contribute not to aerodynamics but to structural effects. In contrast, Dao et al. [45] numerically investigated two-dimensional corrugated flapping wings with the prescribed deformation in accordance with the FWMAV and reported that the leading-edge corrugated wings were beneficial in enhancing aerodynamic performance at a higher angle of attack. The aerodynamic effect of corrugated flapping wings is not fully understood yet.

Corrugation implemented in the chordwise direction generally enforces spanwise flexural rigidity and provides anisotropic rigidity to the wing surface even with an isotropic material. The anisotropy due to corrugation depends on not only the corrugation shape but also the ratio of amplitude of corrugation to plate thickness [33]. Thus, the design of corrugation shape and plate thickness affects both the anisotropic flexural rigidity and the mass of the wing; consequently, it not only changes the static structural characteristics but also the dynamic ones (i.e., natural frequencies and vibrational modes). To reveal the aeroelastic effects of a corrugated flapping wing, a comprehensive parametric study is required because a corrugated cross section simultaneously affects the aerodynamics [45], elasticity [33], and inertia [46] of a flapping wing. However, the effects of corrugation for a flapping wing with passive aeroelastic deformation have not been investigated yet.

Although the anisotropic flexural rigidity of actual insect wings is provided by the vein distribution and cambered cross section in addition to the corrugation, we focus on the aeroelastic effect of corrugation of an insect-sized flapping wing, excluding the veins and cambered airfoil. The objective is not to simulate a realistic insect wing but to numerically investigate the fundamental aeroelastic effects of a corrugated flapping wing in hovering flight. For this purpose, a simplified wing structure and kinematics are constructed by reference of insect wings. However, the size, mass, and material properties of the wing model, which dominate the aeroelastic similarity parameters (namely, Reynolds number, reduced frequency, mass ratio, and natural and flapping frequency ratio [22]) must match those of the insect wings to elicit the aeroelastic effects for an insect-sized flapping wing. Therefore, a baseline structural wing model is constructed in accordance with the size, mass, and material properties of bumblebee wings. Around the baseline, the amplitude of corrugation and the plate thickness are systematically altered over wide ranges, which affects the anisotropic flexural rigidity and mass of the wing in addition to the aerodynamics. Using the results from the parametric study, we discuss the optimal corrugated cross section for an elastic flapping wing in comparison with the structural design of insect wings. The unsteady aeroelastic calculation is based on 3-D Navier–Stokes equation for aerodynamics coupled with a modified mode method for the structure. To validate the numerical method, thrust and natural frequencies are measured using scale-up models for an elastic flapping wing with a corrugated cross section.

II. Numerical Model and Methods

A. Flapping-Wing Kinematics

The three-dimensional coordinate system of a flapping wing is shown in Fig. 1. The *XYZ* system is fixed to the body, and the *xyz* system is fixed to the undeformed starboard wing. The simplified wing kinematics comprises two motions: flapping and feathering. The flapping motion is a rotational oscillation around the body axis (*X*-axis), and the feathering motion is a rotational oscillation around the span axis (*y*-axis) of the wing. Because this study focusses on hovering flight, the stroke plane of the flapping wing (*YZ* plane) was horizontal, and the wing was moved in the same pattern between the up- and downstrokes to cancel the horizontal force (or drag). The flapping angle ϕ can be defined as the angle from the neutral axis (*Y*-axis) of the flapping oscillation to the spanwise axis of the wing. The feathering angle θ can be defined as the angle between the wing chord line and the vertical axis. In this study, the flapping and feathering oscillations applied to the wing base were provided as two simple sinusoidal waves with a phase difference of 90 deg, which are given as follows:

$$\phi_{\text{in}}(t) = -\hat{\phi}_{\text{in}}\cos(2\pi f_{\text{in}}t)$$

$$\theta_{\text{in}}(t) = -\hat{\theta}_{\text{in}}\cos(2\pi f_{\text{in}}t + \pi/2) \tag{1}$$

A baseline model for an insect-sized corrugated flapping wing was developed in accordance with wings of bumblebees (*Bombus terrestris*), which have corrugated cross sections [36]. In accordance with the measured data for a bumblebee [47], the input flapping frequency f_{in} was 150 Hz, and the input flapping amplitude $\hat{\phi}_{\text{in}}$ was 55 deg. The input feathering amplitude $\hat{\theta}_{\text{in}}$ was 45 and 0 deg for the semi-passive or fully passive feathering to simulate both biological and robotic applications. In the recent FWMAVs [1–5], the feathering rotation is not input at the wing base ($\hat{\theta}_{\text{in}} = 0$) and is achieved by fully passive torsional deformation. In contrast, the feathering response of insects is modeled as an input feathering rotation and a passive torsional deformation [17–20, 23, 26, 43] although the exact input amplitude is still unknown. In this study, $\hat{\theta}_{\text{in}}$ was set to 45 deg, at which a rigid flapping wing generates lift close to the maximum [16]. A wing response during a flapping cycle is caused by these input oscillations and aeroelastic deformation. The output flapping and feathering angles are denoted by ϕ_{out} and θ_{out}, respectively, and the deformation angles of flapping and feathering are denoted by ϕ_{def} (= $\phi_{\text{out}} - \phi_{\text{in}}$) and θ_{def} (= $\theta_{\text{out}} - \theta_{\text{in}}$), respectively.

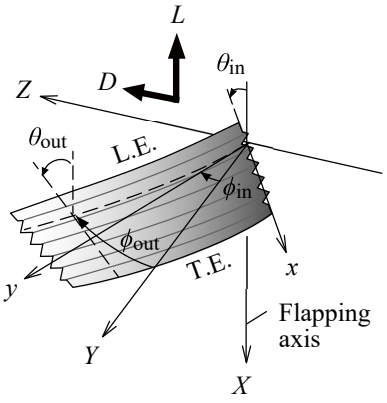

Fig. 1 Coordinate systems of a flapping wing.

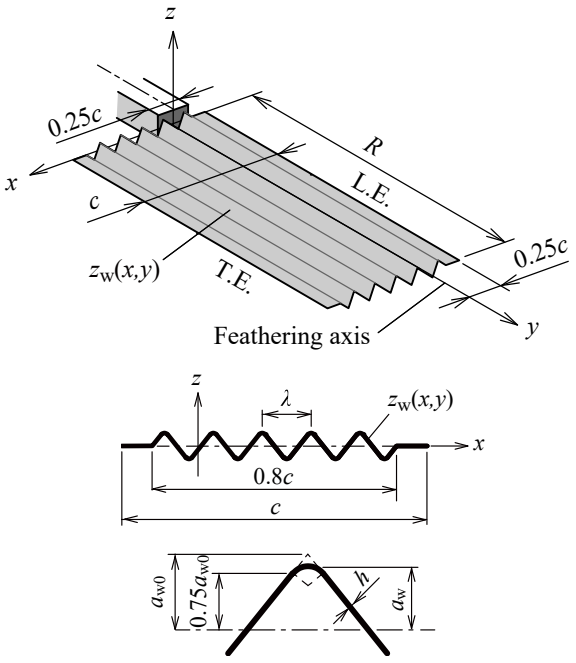

Fig. 2 Planform, support conditions, and corrugated cross section of the model wing.

B. Wing Structural Model

Insect wings are composed of complicated structural elements [33–35]. The hollow veins and extremely thin membrane contribute to the very light-weight structure. The distinguishing vein pattern, inhomogeneous thick distribution, and corrugated cross sections provide the wing with appropriate stiffness and mass distribution, resulting in a preferable aeroelastic deformation during a flapping cycle. In this study, the wing model was simplified as shown in Fig. 2 to elicit fundamental aeroelastic effects of a corrugated cross section. The wing length and mass were set to the averaged data of the bumblebee wings used for the tensile tests of the wings [48]. The averaged semi-span length R is 13.06 mm, and the wing mass m_w is 0.52 mg. The wing had a rectangular planform with the same semi-span length and aspect ratio (= $2R^2/S_{\text{w}}$ = 6.25 [36]) as those of the bumblebee wing (consequently, c = 4.18 mm). Owing to the rectangular planform, the corrugated cross section is quite identical at each span station. The flapping axis was at the wing base, and the feathering axis was located 0.25c away from the leading-edge. The wing was fixedly supported at the wing base with a width of 0.25c around the feathering axis, and the input flapping and

feathering oscillations shown in Eq. (1) were applied to the wing base. The corrugated cross section of the wing was simplified as a triangular wave, similar to previous studies [33,41–45]. Although Dao et al. [45] showed that the corrugations placed on the entire wing chord are not beneficial to enhance the aerodynamic performance, we implemented five waves ($n_w = 5$) with an amplitude of a_{w0} from $0.1c$ to $0.9c$ to minimize a local reinforcement effect for a simple discussion. Consequently, a wave length λ is $0.16c$, which covers the wave length shown in the literature [33] ($0.30c$ for an ichneumon, $0.27c$ for a crane fly, and $0.16c$ for a hoverfly). Furthermore, each 10% chord at the leading- and trailing-edges is flat to minimize the aerodynamic camber effect. Each vertex of the triangular wave was rounded from 75% amplitude to reduce the effect of sharp edges on aerodynamics; thus, the net amplitude is represented as a_w. The rounded vertices are more feasible design in manufacturing than the sharp vertex. The middle surface of the corrugated plate is denoted by $z_w(x, y)$. Because the wing had an isotropic material and a homogeneous thickness h, the anisotropic flexural rigidity of the wing was provided by only the corrugated cross section.

Material properties of the wing were determined so that the balance of elastic and inertial forces of the wing agrees with that of bumblebee wings. Insect wings are composed primarily of cuticle, whose material properties can vary depending on the hydration, sclerotization, and chitin fiber orientation [35]. In our homogeneous wing model, the Young's modulus was set to 3.75 GPa, which is the average of the Young's moduli of the leading-edge vein (5.14 GPa) and of the membrane near the wing tip (2.36 GPa) measured in the tensile tests of the bumblebee's wings [48]. The Poisson's ratio is 0.49, which is commonly used for biomaterials [49]. The density of cuticle is 1200 kg/m^3 [49]. However, when the actual material density is utilized for our homogeneous wing model, the inertial contribution can be overestimated compared with the elastic one because the wing model neglects the complicated inhomogeneous structures (e.g., hollow vein tubes, vein pattern, and thickness distribution). Thus, the material density was modulated so that the flexural rigidity and mass of the baseline wing model were the same as those of the actual wings of bumblebees. The spanwise and chordwise flexural rigidities of the baseline model were determined in accordance with the measurement performed by Combes and Daniel [34] in a cantilever beam bending test for wings of various species of insects. They obtained the regression relations of the spanwise and chordwise flexural rigidities with the size of the insects' wings. Using the regression relationship, the spanwise flexural rigidity (EI_s) for the baseline model was estimated to be 3.05×10^{-6} Nm^2, and the chordwise one (EI_c) was 2.10×10^{-7} Nm^2. When the corrugated wing was regarded as a simple Bernoulli-Euler cantilever beam, as was done in a previous study [34], the spanwise and chordwise flexural rigidities for the triangular-wave cross section without rounded vertices can be given by [33]

$$\frac{EI_s^{crg}}{EI_s^{flat}} = 1 - \frac{n_w\lambda}{c} + \frac{n_w\lambda}{c}\sqrt{1+\left(\frac{4a_{w0}}{\lambda}\right)^2}\left\{1+\left(\frac{4a_{w0}}{\lambda}\right)^2+\left(\frac{2a_{w0}}{h}\right)^2\right\} \tag{2}$$

$$\frac{EI^{crg}}{EI_c^{flat}} = \frac{1}{1+(n_w\lambda/c)\left\{\sqrt{1+(4a_{w0}/\lambda)^2}-1\right\}} \tag{3}$$

where $EI_s^{flat} = Ech^3/12$ and $EI_c^{flat} = ERh^3/12$, which denote the flexural rigidities for a flat plate. In accordance with Eqs. (2) and (3) considering rounded vertices, $h = 40.1$ μm and $a_w/c = 2.62\%$ are necessary for the baseline model to attain both the estimated spanwise and chordwise flexural rigidities. The a_w/c estimated above agrees well with the amplitude of corrugation of 3% used in previous studies [41–45], which is the average of various insects' wings [33]. Using the estimated h and a_w/c for the baseline model and the mass of the bumblebee's wing m_w, the apparent material density was estimated to be 202 kg/m^3. In the numerical simulation, the apparent material density of wing ρ_w was approximately set to 200 kg/m^3.

Around the baseline model based on the bumblebee's wing determined above, the two parameters, h and a_w, were varied systematically to investigate the aeroelastic effects of corrugated flapping wings. The amplitude of the sharp triangle wave a_{w0} was set to 0, 1, 2, 3, 4, and 5% c. These wings are named Flat, Crg1, Crg2, Crg3, Crg4, and Crg5, respectively. As a result of the rounded vertices, the net amplitude a_w was reduced to 0.87, 1.74, 2.58, 3.41, 4.23% c, respectively. The structural parameters for each model are summarized in Table 1. The vertex angles of the respective cross sections were 152, 127, 106, 90, and 77.3

deg, respectively, which covered the range of values of the seven species of insects, 102–160 deg, measured by Rees [33]. As shown in Eqs. (2) and (3), the variations of h and a_w affect the ratio of the spanwise and chordwise flexural rigidities in addition to the wing mass; consequently, they change the natural frequencies and vibrational modes of the wing. In this study, h was selected so that the ratio of the first natural frequency to the input flapping frequency, $f_1^* = f_1/f_{in}$, was in the range of 1.0–4.5, as shown in Table 1. This frequency range covers the natural flyers at $1.25 < f_1^* < 3.33$ [22] and is enough to demonstrate the aeroelastic characteristics of the insect-sized flapping wing. As described subsequently in Sec. IV, considerable deformation occurred at $f_1^* < 1$ whereas the wing response approached that of the rigid wing at $f_1^* > 4.5$.

Table 1 Structural parameters in the range of $f_1^* = 1$–4.5

Wing	a_w/c, %	f_1^*	h, μm	$2a_w/h$	$4a_w/\lambda$	EI_S^{crg}/EI_S^{flat}	EI_C^{crg}/EI_C^{flat}
Flat	0	1.0	42	0	0	1	1
		4.5	188				
Crg1	0.87	1.0	9	8.1	0.22	52	0.98
		4.5	182	0.40		1.2	
Crg2	1.74	1.0	6	24	0.43	472	0.93
		4.5	150	0.94		2.0	
Crg3	2.58	1.0	4	54	0.65	2510	0.87
		4.5	90	2.4		6.4	
Crg4	3.41	1.0	3	95	0.85	8370	0.80
		4.5	50	5.7		32	
Crg5	4.23	1.0	3	117	1.1	13800	0.74
		4.5	30	9.1		84	

C. Numerical Methods

Unsteady aeroelastic responses and aerodynamic characteristics of the corrugated flapping wings were calculated using the 3-D Navier–Stokes solver coupled with the equations of motion of the wing in modal space. Prior to the unsteady aeroelastic analysis, modal analysis using the finite element method (FEM) was conducted for the wing models using a commercial structural analysis software, ANSYS 18.0. Two-dimensional four-nodes shell elements (SHELL181) were employed on the corrugated wing surface. The wing was rigidly supported at the wing base, as shown in Fig. 2. The k-th natural frequency f_k, the mode shape $\Phi_k(x, y)$, and the modal mass M_k were obtained through modal analysis, and the in-plane vibrational modes were ignored. The number of elements was 187 in the spanwise direction, and 61 in the chordwise direction for Flat, 76 for Crg1, and 96 for Crg2–Crg5, which were based on the mesh convergence analysis. We confirmed that the modal characteristics calculated using the 2-D shell elements agree well with those obtained using 3-D solid elements for the range of h and a_w used in this study. The comparison of the two results are shown in Appendix.

In the unsteady aeroelastic analysis, the out-of-plane displacement w of the neutral surface of the corrugated plate comprises the forced displacement w_{in} and the elastic deflection w_d, as follows:

$$w(x, y, t) = w_{in}(x, y, t) + w_d(x, y, t) \tag{4}$$

In the mode method, the elastic deflection is represented as a superposition of the modes ($N = 3$) and is given by

$$w_d(x, y, t) = \sum_{k=1}^{N} \Phi_k(x, y)\xi_k(t) \tag{5}$$

where ξ_k is the kth modal coordinate. The equation of motion for the wing is represented in modal space as follows:

$$\ddot{\xi}_k + 2\pi(f_k^2/f_{\text{in}})g_k\dot{\xi}_k + (2\pi f_k)^2\xi_k = \frac{1}{M_k}\iint_S (F_n\Phi_k - \rho_w h\Phi_k\ddot{w}_{\text{in}})dxdy \tag{6}$$

where g_k is the structural damping coefficient ($g_k = 0.01$), and F_n is the aerodynamic force normal to the wing, which is obtained by solving the 3-D Navier–Stokes equations with computational fluid dynamics (CFD) at each time step. The out-of-plane acceleration of the wing surface caused by the forced-oscillation shown in Eq. (1) is given by

$$\ddot{w}_{\text{in}}(x,y,t) = x\left(\dot{\phi}_{\text{in}}^2 \sin\theta_{\text{in}} \cos\theta_{\text{in}} - \ddot{\theta}_{\text{in}}\right) + y\ddot{\phi}_{\text{in}} \cos\theta_{\text{in}} - z_w\left(\dot{\phi}_{\text{in}}^2 \cos^2\theta_{\text{in}} + \dot{\theta}_{\text{in}}^2\right) \tag{7}$$

By solving Eq. (6) using an implicit time-integration, the modal coordinates can be obtained at each time step.

The conventional representation of deflection in the linear mode method shown in Eq. (5) distorts the corrugated cross-sectional shape with increasing deflection because the large rotation in geometric nonlinearity is neglected. In this study, the representation of the chordwise deflection was modified so that the chordwise arc length of the neutral surface of plate maintained its original length after deflection. The chordwise angle of deflection ζ_x is represented as a superposition of the chordwise gradient of the vibrational modes, as follows:

$$\zeta_x(x,y) = \sum_{k=1}^{N} \frac{\partial\Phi_k}{\partial x}\xi_k \tag{8}$$

When the chordwise arc length is always maintained after deflection, the displacements of the wing section can be represented as an integration of the directional cosine of the line element ds from the elastic axis ($x = 0$), as shown in Fig. 3. In contrast, the displacement in the spanwise direction is still based on the conventional mode method because the spanwise bending is generally much smaller than the chordwise bending for flapping wings. Therefore, the displacements of the wing sections in the x- and z-directions, u_d and w_d, respectively, are updated as follows:

$$\begin{aligned} u_d(x,y) &= \int_0^x \cos\{\zeta_x(s,y)\}\,ds - x \\ w_d(x,y) &= w_{ea}(0,y) + w_r(x,y) = \sum_{i=1}^{N} \Phi_i(0,y)\,\xi_i + \int_0^x \sin\{\zeta_x(s,y)\}\,ds \end{aligned} \tag{9}$$

Once the neutral surface of the wing is determined, the corrugated cross section after deflection can be provided such that the height of the corrugation, z_w, remains normal to the neutral surface, as shown in Fig. 3.

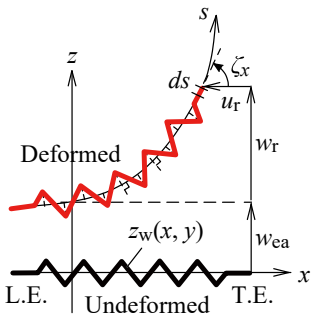

Fig. 3 Bending and large rotation of a corrugated cross section.

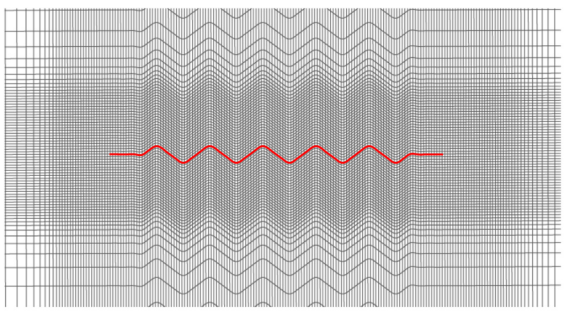

Fig. 4 CFD grid around the airfoil Crg3.

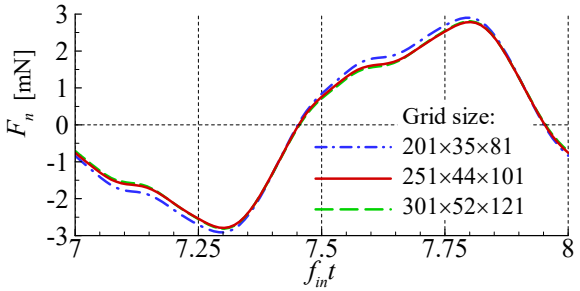

Fig. 5 Comparison of the CFD grids. Time histories of fluid force normal to the wing surface during a flapping cycle for Crg5 with $f_1^* = 4.5$ when $\hat{\theta}_{in} = 45$ deg.

The modified expression shown in Eqs. (8) and (9) approximately considers the nonlinear large rotation in the chordwise direction. In contrast, the effects of large rotation in flapping is smaller than that in feathering. According to previous experimental and numerical studies [9–12], even if the flapping rotation is linearized (i.e., $\sin\phi \approx \phi$), the aerodynamic force and power for the numerical results agree well with the experimental results (2% error in the mean lift and 7% in the mean power when $\hat{\phi}_{in} = 60$ deg for a rigid flapping wing [12]) because the rotational effect of flapping is small. To reduce the computational cost, the flapping and spanwise bending were linearized, whereas large rotation was considered in the feathering and chordwise bending, as follows:

$$\begin{Bmatrix} X \\ Y \\ Z \end{Bmatrix} = \begin{bmatrix} \cos\theta_{in} & 0 & \sin\theta_{in} \\ 0 & 1 & 0 \\ -\sin\theta_{in} & \phi_{in} & \cos\theta_{in} \end{bmatrix} \begin{Bmatrix} x + u_r - z_w \sin\zeta_x \\ y \\ w_d + z_w \cos\zeta_x \end{Bmatrix} \tag{10}$$

The flow around the deformed flapping wing represented in Eq. (10) was solved using an in-house 3-D Navier–Stokes solver, which is based on the finite difference method with an implicit-time-integration scheme [50] and a total variation dimisishing scheme [51]. The details of the numerical method are described in previous studies [9,11]. The Reynolds number was 1210, defined using the chord length and the reference velocity defined as the mean flapping velocity ($U_{ref} = 4f_{in}\hat{\phi}_{in}r_{ref}$) at the radius of gyration r_{ref} ($= R/\sqrt{3}$). Hence, no turbulence model was employed. The reduced frequency ($= \pi f_{in}c/U_{ref} = \pi c/4\hat{\phi}_{in}r_{ref}$) was 0.453. The Reynolds number and the reduced frequency are almost the same as those of bumblebees [47]. The computational domain was $30c$ in the flow-direction (X) and the stroke-direction (Z), and $3R$ in the spanwise direction (Y). The symmetrical boundary was applied on the X-Z plane. At the wing surface, the no-slip conditions were given. A body-fitted H-H grid was arranged around the deformed flapping wing with a zero thickness at each time step, which were moved together with the elastic flapping wing on the basis of the geometric conservation law [52]. The grid points were 251 (125 on the wing) in the chordwise direction, 44 (31 on the wing) in the spanwise direction, and 101 in the stroke direction (normal to the wing surface). The time step was 1/4704 of a flapping cycle. The grid around the airfoil of Crg3 are shown in Fig. 4.

To investigate the mesh dependency, we calculated the unsteady aerodynamic forces for an elastic flapping wing of Crg5 using a coarse grid (201 × 35 × 81) and a fine grid (301 × 52 × 121) in addition to the presently employed grid (251 × 44 × 101). The time histories of aerodynamic force normal to the wing surface, F_n, for the three grids are shown in Fig. 5. There is no difference in the aerodynamic force between the present and fine grids. In addition, we confirmed that there is no difference in the aerodynamic force and elastic response between the present time step and a fine time step of 1/9408 of a flapping cycle.

D. Evaluation of Aeroelastic Characteristics

The aerodynamic characteristics of an elastic flapping wing (i.e., mean lift $\bar{L}$, mean power $\bar{P}$, and hovering efficiency η) were evaluated in the eighth flapping cycle in which the aerodynamic force and elastic deformation were in a steady oscillation. The flapping and feathering powers required at the wing base are denoted by P_ϕ ($= Q_\phi\dot{\phi}_{in}$) and P_θ ($= Q_\theta\dot{\theta}_{in}$), where Q_ϕ and Q_θ

are the flapping and feathering torques at the wing base, respectively. We employed the assumption that the input flapping and feathering motions are actuated by separate actuators or muscles, and these actuators or muscles cannot store and utilize negative power [13]. Accordingly, the total mean power $\bar{P}^+$ is represented as follows:

$$P^+_{\phi,\theta}(t) = \mathrm{MAX}\{P_{\phi,\theta}(t), 0\}, \qquad \bar{P}^+ = \mathrm{mean}\{P^+_{\phi}(t)\} + \mathrm{mean}\{P^+_{\theta}(t)\} \tag{11}$$

Note that the mean inertial power is not zero during a flapping cycle because of the assumption and is comparable in magnitude to the mean aerodynamic power. Thus, a light-weight structure is critical to reduce the total power.

We evaluated the hovering efficiency η, or a figure-of-merit, of a flapping wing based on the ideal momentum theory, which is the mean power induced in the air divided by the mean required power [14], which is given by

$$\eta = \frac{\bar{L}^{3/2}}{\bar{P}^+\sqrt{2\rho_a R^2 \hat{\phi}_{\mathrm{out}}}} \tag{12}$$

where ρ_a is the air density. In general, the lift generated by a flapping wing is proportional to the square of the flapping amplitude, and the aerodynamic power is proportional to the cube. Therefore, the change in the flapping amplitude does not affect the hovering efficiency in terms of the aerodynamic contribution [15]. However, for an elastic flapping wing, the flapping amplitude affects the hovering efficiency in terms of the inertial power.

The wing response was evaluated as the flapping and feathering angles at the reference span station (r_{ref}) and the first modal coordinate. The time histories of the flapping and feathering angles and the first modal coordinate are expanded in the Fourier series as follows:

$$\phi_{\mathrm{out}}(t) = -\sum_{j=1}^{\infty} \hat{\phi}_j \cos(2\pi j f_{\mathrm{in}} t + \alpha_j)$$

$$\theta_{\mathrm{out}}(t) = -\sum_{j=1}^{\infty} \hat{\theta}_j \cos(2\pi j f_{\mathrm{in}} t + \beta_j) \tag{13}$$

$$\xi_1(t) = -\sum_{j=1}^{\infty} \hat{\Xi}_{1,j} \cos(2\pi j f_{\mathrm{in}} t + \gamma_{1,j})$$

where α, β, and γ are the phase lead with respect to the input flapping oscillation. In this study, the aeroelastic response was evaluated with the amplitudes and phases of the first harmonics because the first harmonics are considerably predominant over the others; that is, $\hat{\phi}_{\mathrm{out}} \approx \hat{\phi}_1$ and $\hat{\theta}_{\mathrm{out}} \approx \hat{\theta}_1$. The phase lead of the feathering oscillation relative to the flapping oscillation is defined as $\psi_{\mathrm{F/F}} = \beta_1 - \alpha_1$. The phase lag of the output relative to the input is defined as $\psi_{\mathrm{I/O}} = -\gamma_{1,1}$.

III. Experiments and Numerical Validation

The numerical methods for CFD and aeroelastic analysis were validated for rigid flat flapping wings [9–12] and for elastic flat flapping wings [53] without corrugated airfoils. To validate the aeroelastic simulation described in Sec. II.C for the elastic corrugated flapping wings, we measured the natural frequencies and the mean lift using scale-up models. The experimental wing model had a scale-up rectangular planform (R = 80 mm and c = 25.6 mm) with the same aspect ratio as the numerical model. The wing was made of a polyethylene terephthalate sheet (Toray Lumirror®, Young's modulus: 6.0 GPa, Poisson's ratio: 0.35, and ρ_{w} = 1400 kg/m^3). The triangular-waved cross section (a_{w0}/c = 3% and n_{w} = 3 from 0.1c to 0.9c) was developed via hot-press molding. Thus, the vertices of the triangular wave were spontaneously rounded. The net a_{w}/c of the wings was 2.39%, which is almost the same as the numerical models of the baseline (a_{w}/c = 2.62%) and Crg3 (a_{w}/c = 2.58%) with the

rounded vertices. For comparison, three wing models were developed: a flat wing with h = 188 μm (named Flat-h188), a corrugated wing with h = 188 μm (Crg-h188), and a corrugated wing with h = 120 μm (Crg-h120). The thicknesses were selected from the available films and $2a_w/h$ is 6.51 and 10.2, respectively, which cover the range of the numerical model shown in Table 1. The two resulting corrugated wings had a chordwise-bending mode due to spanwise reinforcement by corrugation. The wings were fixed at the wing base from 0 to 0.25c, as shown in Fig. 6a.

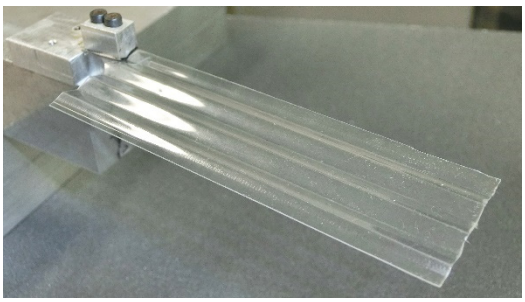

a) Photograph of the corrugated wing

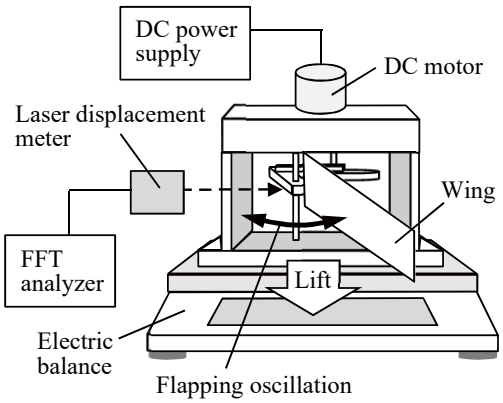

b) Lift measurement system

Fig. 6 Experimental apparatus and wing model.

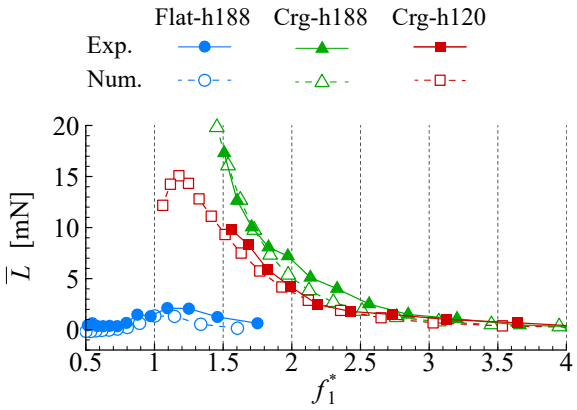

Fig. 7 Mean lift with respect to the natural frequency ratio for experimental and numerical results.

In measurement of natural frequencies, a small sinusoidal oscillation was applied to the wing base. By sweeping the oscillated frequency, the responses of the wing were measured using laser displacement measurements and a fast Fourier transform (FFT) analyzer. Using the measured frequency spectrum, the first and second natural frequencies were identified. The natural frequencies were measured using a single specimen in each model. In addition, modal analysis was conducted for the experimental model using FEM with the element size of 0.5 mm. The first and second natural frequencies of the experimental and numerical results are shown in Table 2. The experimental and numerical natural frequencies show good agreement.

The lift measurement system is shown in Fig. 6b. The wing was fixed at the wing base 30 mm apart from the flapping axis of the flapping mechanical apparatus and was oscillated horizontally at $\hat{\phi}_{in}$ = 21.4 deg. These parameters were different from the numerical model because of the limitation of the mechanical apparatus. The wing was mounted on the apparatus such that the leading-edge of the wing was directed downward to minimize the interaction between the wake and the measurement system. The time-averaged downward lift at several input frequencies was measured using an electric balance (BX3200H, Shimadzu Corporation). The mean lift was measured and averaged with three specimens in each model. Additionally, aeroelastic analyses for the experimental models were conducted using the same grid described in Sec. II.C. The mean lift with respect to the input frequency for the experimental and numerical results is shown in Fig. 7, where the horizontal axis f_1^* is the ratio of the first natural frequency to the input flapping frequency. The numerical results quantitatively agree well with the

experimental results, indicating the validity of our aeroelastic analysis. In the experiment, structural failure occurred at the wing bases of Crg-h188 and Crg-h120 at $f_1^* < 1.5$ due to the large deformation.

Table 2 Natural frequencies of the experiment and numerical results

Wing	f_1, Hz		f_2, Hz	
	Exp.	Num.	Exp.	Num.
Flat-h188	9	8	50	45
Crg-h188	26	27	73	76
Crg-h120	22	21	64	63

IV. Results

A. Structural Characteristics

In this study, the plate thickness h for each wing model was varied, which consequently modulates the natural frequency or the balance of elastic to inertial forces. Figure 8 shows the relation of f_1^* to the wing mass, which is proportional to h. The mass ratio m_w^* is defined as $m_w/\rho_a S_w c$ based on the literature [54]. The structural characteristics of the wings can be coordinated by changing f_1^* instead of h because f_1^* has a one-to-one relation with h and because the aeroelastic responses of the flapping wings are dominated by the first mode. Figure 8 shows that the corrugated cross section with a higher a_w can reduce the weight with the natural frequency kept constant. The wing masses of Crg1–Crg4 asymptotically approach that of Crg5 with decreasing f_1^* and that of Flat with increasing f_1^*. The weight reduction effect due to corrugation is weaker for the wings with a higher a_w or a smaller f_1^* (i.e., a thinner h).

Figure 9a shows the representative first mode shapes at $f_1^* = 1.5$, 3.0, and 4.5. The first mode shape is categorized into a spanwise-bending mode, a chordwise-bending mode, or a mixture of both. To quantitatively evaluate the mode shapes, the representative gradient direction of mode shape was calculated, which is the average in the range of 0.5–1.0c at r_{ref}. The gradient directions of the first modes for the corrugated wings are shown in Fig. 9b, where the spanwise and chordwise directions denote 0 and 90 deg, respectively. The mode shape of Flat is dominated by the spanwise bending and is independent of h (i.e., f_1^*), while the mode shape of Crg5 is dominated by the chordwise-bending mode and does not change significantly with f_1^*. The mode shapes of Crg1–Crg4 asymptotically approach that of Flat with increasing f_1^* and that of Crg5 with decreasing f_1^*, as well as the tendency of the wing mass, as shown in Fig. 8. These results indicate that the wings with a chordwise-bending mode have a lighter weight than those with a spanwise-bending mode when the wings with the same f_1^* are compared.

According to Eqs. (2) and (3), the spanwise flexural rigidity ratio, EI_S^{crg}/EI_S^{flat}, depends on $2a_w/h$ and $4a_w/\lambda$, whereas the chordwise one, EI_C^{crg}/EI_C^{flat}, depends only on $4a_w/\lambda$. As shown in Table 1, $4a_w/\lambda$ is in the order of magnitude of 0.1–1, whereas $2a_w/h$ varies considerably with h. Therefore, the effect of $4a_w/\lambda$ can be neglected in comparison with that of $2a_w/h$. Actually, EI_C^{crg}/EI_C^{flat} does not significantly vary with a_w and is approximately equal to the ratio of the curve length of the corrugated cross section to the chord line (i.e., the wing area ratio of the flat to the corrugated wing). In contrast, EI_S^{crg}/EI_S^{flat} varies considerably with $2a_w/h$. Therefore, the corrugation reinforcement is considered to be approximately dependent on only $2a_w/h$ and is effective for only the spanwise flexural rigidity. For the flat wing, spanwise bending appears in the first mode because the spanwise bending stiffness (EI_S/R) is smaller than the chordwise one (EI_C/c) due to the aspect ratio ($R > c$). For corrugated wings, the ratio of the spanwise to chordwise bending stiffness varies primarily with $2a_w/h$. When the spanwise bending stiffness becomes larger than the chordwise one due to the corrugation reinforcement with increasing $2a_w/h$, chordwise bending appears in the first mode. Once the chordwise bending is predominant in the first mode, the further increase of $2a_w/h$ no longer varies the first mode shape because $2a_w/h$ is not effective for the chordwise reinforcement; therefore, the structural characteristics are similar among the corrugated wings with increasing $2a_w/h$ (e.g., Crg2–Crg5 at a smaller f_1^*). Conversely, as $2a_w/h$ decreases, the corrugation reinforcement does not work, and the structural characteristics of the corrugated wing become similar to those of the flat wing (e.g., Crg1 at a higher f_1^*).

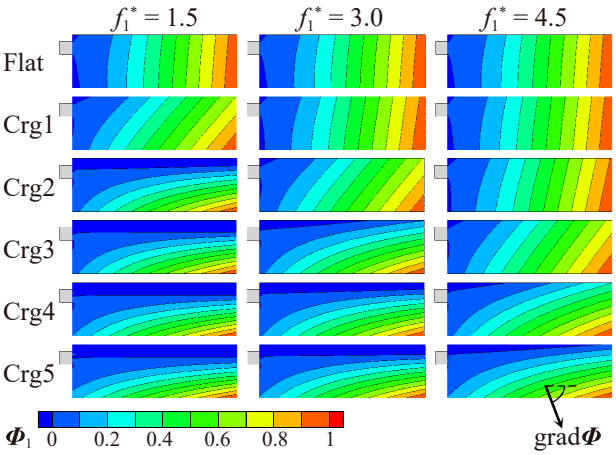

a) Representative first mode shapes

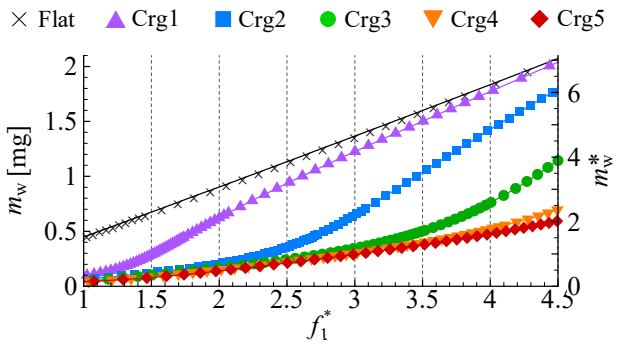

Fig. 8 Wing mass with respect to the natural frequency ratio.

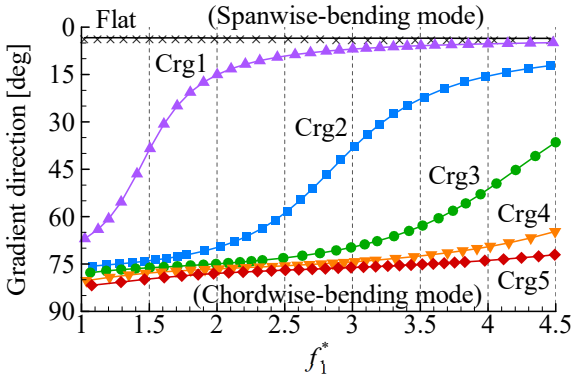

b) Gradient direction of the first mode shape

Fig. 9 Variation of mode shapes with respect to the natural frequency ratio.

B. Aerodynamic and Aeroelastic Characteristics

Prior to discussing aeroelastic characteristics, aerodynamic characteristics of the rigid corrugated wings are discussed. Table 3 shows the mean lift, mean power, and hovering efficiency of the rigid corrugated wings divided by those of Flat when $\hat{\theta}_{in}$ = 45 deg. Note that the power shown in Table 3 denotes the aerodynamic power without the inertial power. The mean lift slightly decreases with increasing height of corrugation, whereas the aerodynamic power slightly increases; consequently, the hovering efficiency decreases with the height of corrugation. These tendencies agree with a previous study on rigid corrugated flapping wings [41].

Table 3 Aerodynamic characteristics of rigid wing models when $\hat{\theta}_{in}$ = 45 deg

	Crg1	Crg2	Crg3	Crg4	Crg5
$\bar{L}_{crg}/\bar{L}_{flat}$	1.00	0.98	0.95	0.90	0.86
$\bar{P}_{a,crg}/\bar{P}_{a,flat}$	1.00	1.01	1.02	1.02	1.02
η_{crg}/η_{flat}	0.99	0.95	0.90	0.84	0.77

Next, aerodynamic characteristics of the elastic corrugated wings are discussed. Figure 10 shows the hovering efficiency η with respect to f_1^* when $\hat{\theta}_{in}$ = 45 and 0 deg. Although the calculation was conducted in the range of $1 \le f_1^* \le 4.5$, a converged solution was not obtained in some cases when f_1^* was small because of a considerable deformation and/or excitation of the

high-order modes. However, this is inconsequential for our discussion because these cases considerably diminish lift (as subsequently shown in Figs. 15a and 17a) and are at a high risk for structural failure. The aerodynamic characteristics and wing responses when the wing models have respective peaks of η are shown in Table 4. The tendency of η with respect to f_1^* is classified into two groups: Flat–Crg1 and Crg3–Crg5. The former group has a lower a_w and a peak of η at $f_1^* < 2$, whereas the latter has a higher a_w and a peak of η at $f_1^* > 2$. Each group has peaks of η at almost the same f_1^* when $\hat{\theta}_{in} = 45$ and 0 deg, respectively. The peak value of η decreases with increasing a_w for Crg3–Crg5, while it increases with a_w for Flat–Crg1. Crg2 has an intermediate tendency between the two groups. Crg2 has a peak of η at $f_1^* = 2.6$ between the two groups when $\hat{\theta}_{in} = 45$ deg, which is the maximum η among all the wings. When $\hat{\theta}_{in} = 0$ deg, Crg2 has two peaks of η at $f_1^* = 2.1$ like Crg3–Crg5 and $f_1^* = 1.4$ like Flat–Crg1. Although the peaks of η of Crg1 and Crg2 at $f_1^* < 2$ are larger than those of Crg2–Crg5 at $f_1^* > 2$, the corresponding lifts of Crg1 and Crg2 are extremely smaller than those of Crg2–Crg5, which means that the peaks of η at $f_1^* < 2$ are not a reasonable solution. Thus, Crg2 at $f_1^* = 2.1$ and Crg3 at $f_1^* = 2.3$ are regarded as optimal wings when $\hat{\theta}_{in} = 0$ deg. In summary, the optimal wing is Crg2 ($a_w/c = 1.7\%$) with $f_1^* = 2.6$ and $m_w^* = 1.5$ when $\hat{\theta}_{in} = 45$ deg, and Crg2–Crg3 ($a_w/c = 1.7$–2.6%) with $f_1^* = 2.1$–2.3 and $m_w^* = 0.7$–0.8 when $\hat{\theta}_{in} = 0$ deg. The optimal wings have a mode shape which asymptotically approaches the chordwise-bending mode of Crg4 and Crg5, as shown in Fig. 9. In contrast, the baseline model based on the insect wings has $a_w/c = 2.6\%$, $f_1^* = 3.6$ and $m_w^* = 1.9$. In comparison between the optimal results and the baseline, the optimal wings are close to the baseline model. This indicates that insect wings have structural characteristics which are similar to the optimal design although the wing design of insects is slightly conservative. Furthermore, the results show that the corrugation is aeroelastically effective in providing the appropriate anisotropic stiffness and light-weight structure for insect wings.

Figure 11 shows the time histories of the response flapping and feathering motions during a flapping cycle for the wings with a peak η. In addition, the sequences of wing motion in the upstroke for Crg2 with a peak η are shown in Fig. 12. The waveforms of wing motions are also classified into two groups. The response feathering motions for the wings with a higher a_w and a peak η at $f_1^* > 2$ are similar trapezoidal waves, whereas those for the wings with a lower a_w and a peak η at $f_1^* < 2$ are similar sinusoidal waves. According to a previous study [12], a trapezoidal feathering motion enhances lift and efficiency more than a sinusoidal one. In the next chapter, we discuss the optimal corrugated flapping wing from the perspectives of the aeroelastic responses and the structural characteristics.

Table 4 Aeroelastic characteristics with the maximum η

$\hat{\theta}_{in}$ deg	Wing	f_1^*	m_w^*	η	$\bar{L}$ mN	$\hat{\phi}_{out}$ deg	$\hat{\theta}_{out}$ deg	$\psi_{I/O}$ deg
45	Flat	1.9	3.0	0.15	1.8	69	47	106
	Crg1	1.9	2.0	0.17	1.6	65	55	111
	Crg2	2.6	1.5	0.20	1.2	60	60	105
	Crg3	3.1	1.3	0.19	1.0	58	60	103
	Crg4	3.3	1.3	0.18	1.0	57	59	103
	Crg5	3.3	1.2	0.16	0.9	56	59	103
0	Flat	1.0	1.6	0.01	0.2	36	8	126
	Crg1	1.2	0.5	0.20	0.5	41	65	98
	Crg2	1.4	0.4	0.17	0.5	55	70	94
		2.1	0.8	0.16	1.3	60	51	113
	Crg3	2.3	0.7	0.16	1.1	59	53	113
	Crg4	2.2	0.6	0.15	1.0	57	54	114
	Crg5	2.3	0.7	0.14	0.9	56	51	117

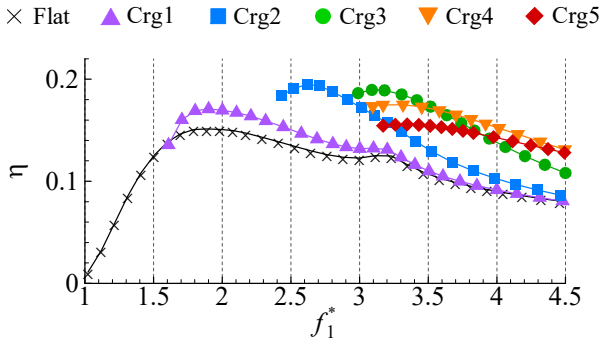

a) θ_{in} = 45 deg

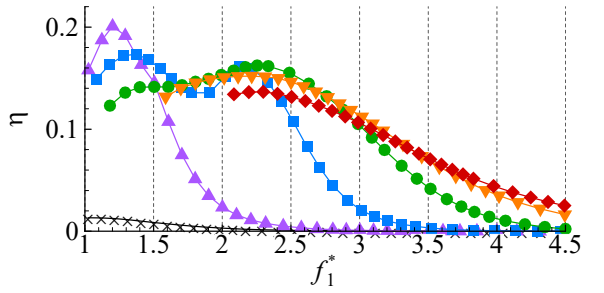

b) θ_{in} = 0 deg

Fig. 10 Hovering efficiency with respect to the natural frequency ratio.

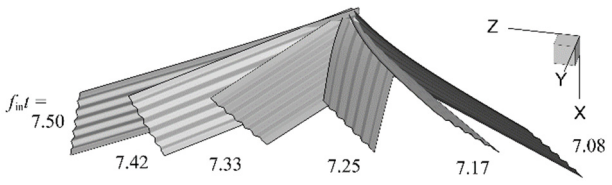

a) Crg2 at f_1^* = 2.6 when $\hat{\theta}_{in}$ = 45 deg

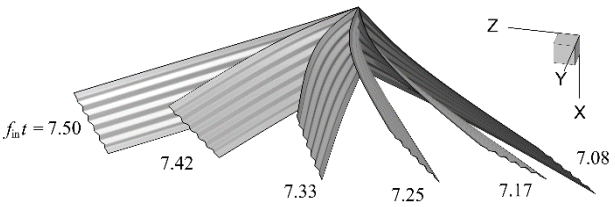

b) Crg2 at f_1^* = 2.1 when $\hat{\theta}_{in}$ = 0 deg

Fig. 12 Wing motion sequences in the upstroke for Crg2 with the maximum η.

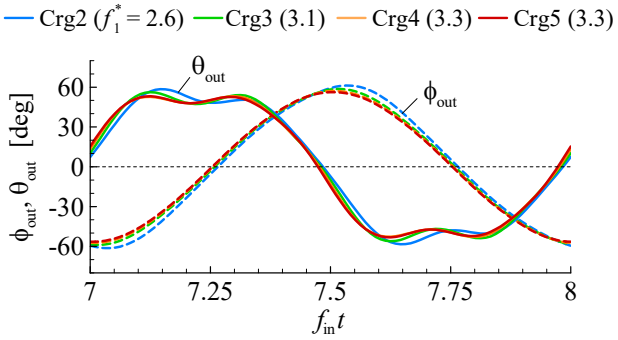

a) Crg2–Crg5 when $\hat{\theta}_{in}$ = 45 deg

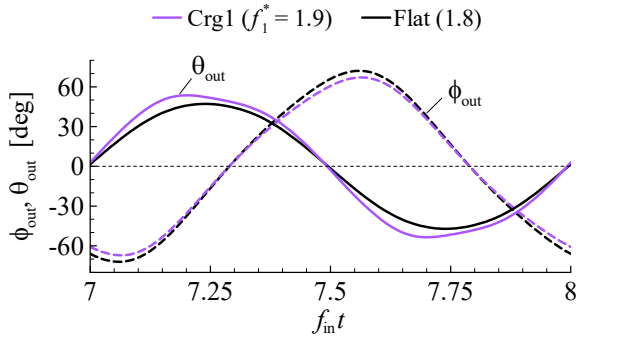

b) Crg1–Flat when $\hat{\theta}_{in}$ = 45 deg

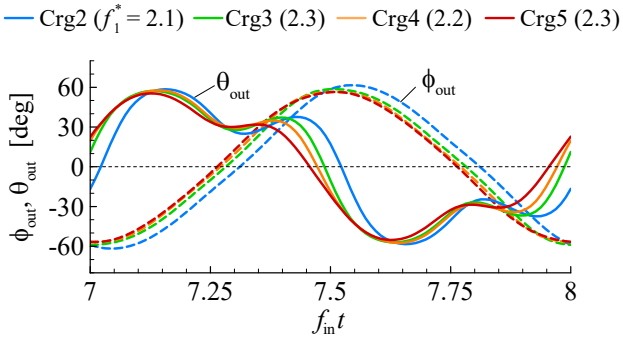

c) Crg2–Crg5 when $\hat{\theta}_{in}$ = 0 deg

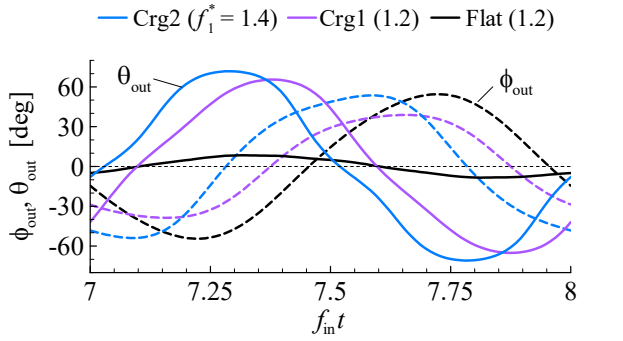

d) Crg2–Flat when $\hat{\theta}_{in}$ = 0 deg

Fig. 11 Time histories of response flapping and feathering motions during a cycle at r_{ref} of each wing with the maximum η.

V. Discussion

A. Aeroelastic Responses in Semi-Passive Feathering

Figures 13a and 13b show the response amplitudes of flapping and feathering motions at r_{ref} with respect to f_1^* when $\hat{\theta}_{in}$ = 45 deg. Figures 13c and 13d show the phase lag between the input and output oscillations, $\psi_{I/O}$, and the phase lead of the feathering motion relative to the flapping motion, $\psi_{F/F}$. First, we focus on the responses at $f_1^* > 2$. A decrease in f_1^* (i.e., a decrease of h) reduces the flexural rigidity of the wing in both the spanwise and chordwise directions, which consequently increases the quasi-static elastic deformation. Moreover, a further decrease in f_1^* approaching the resonance ($f_1^* = 1$) adds a dynamic elastic deformation to the response. As shown in Figs. 13a and 13b, for the wings with the spanwise-bending mode (i.e., Flat and Crg1), $\hat{\phi}_{def}$ and $\hat{\phi}_{out}$ increase with decreasing f_1^*, whereas $\hat{\theta}_{def}$ and $\hat{\theta}_{out}$ do not change. Similarly, for the wings with the chordwise-bending mode (i.e., Crg3–Crg5), $\hat{\theta}_{def}$ and $\hat{\theta}_{out}$ increase with decreasing f_1^*, whereas $\hat{\phi}_{def}$ and $\hat{\phi}_{out}$ do not change. For Crg2, $\hat{\theta}_{def}$ and $\hat{\theta}_{out}$ remarkably increase at $f_1^* = 3.0$ to 2.4, which is attributed to the drastic changes in the mode shape from the spanwise to chordwise-bending directions, as shown in Fig. 9b. Next, we focus on the responses at $f_1^* < 2$. For Flat, $\hat{\phi}_{out}$ decreases with decreasing f_1^* despite the increase in $\hat{\phi}_{def}$. This is caused by the rapid shift in $\psi_{I/O}$ at $f_1^* < 2$ due to resonance, as shown in Fig. 13c. The spanwise bending with large phase lag relative to the input flapping oscillation not only reduces the flapping amplitude but also causes a large figure-of-eight stroke deviation at the wing tip in the semi-passive feathering motion, as shown in Fig. 14a, resulting in lift reduction and a slight decrease in the efficiency [16]. For Crg1, both the rapid shift in $\psi_{I/O}$ and the mode conversion from the spanwise to chordwise-bending directions occur at the same time at $f_1^* < 2$, which causes both a reduction in $\hat{\phi}_{out}$ and an increase in $\hat{\theta}_{out}$. In the semi-passive feathering motion, $\psi_{F/F}$ is mainly dominated by the input $\psi_{F/F}$ of 90 deg when $\psi_{I/O}$ is small at f_1^* far from 1.0, as shown in Figs. 13c and 13d. However, the increase in $\psi_{I/O}$ with f_1^* decreasing and approaching the resonance also causes a drastic increase in $\psi_{F/F}$ apart from the input of 90 deg, which significantly reduces the efficiency [12,16] for Flat and Crg1, as shown in Fig. 10a.

The mean lift with respect to f_1^* is shown in Fig. 15a. At $f_1^* = 4.5$, where the wing is considered to be rigid, the small difference in lift among Flat–Crg5 is attributed to the aerodynamic effect of the corrugated airfoils and agrees with those in the rigid cases shown in Table 3. The lift for the wings with the spanwise-bending mode (e.g., Flat and Crg1) increases with decreasing f_1^* but decreases considerably at $f_1^* < 2$. This tendency of lift agrees with that of $\hat{\phi}_{out}$ shown in Fig. 13a because lift is proportional to the square of $\hat{\phi}_{out}$. In contrast, lift for the wings with the chordwise-bending mode (e.g., Crg3–Crg5) slightly varies with f_1^*. A small peak of Crg3–Crg5 appears at $f_1^* = 3.4$–4.0 when $\hat{\theta}_{out}$ reaches 54–55 deg with the appropriate chordwise bending. The mean total power with respect to f_1^* are shown in Fig. 15b. As shown in the rigid case, the effect of corrugation on the aerodynamic power is small. Nevertheless, at $f_1^* = 4.5$, where the wing responses are almost the same among Flat–Crg5, there is a remarkable difference in the total power among the wing models. This indicates that the difference in the total power is mainly attributed to that in the inertial power, or the wing mass. The total power tends to decrease with decreasing f_1^*, which is similar to the tendency of m_w, as shown in Fig. 8. At $f_1^* < 3$, the total power of Flat and Crg1 increases with decreasing f_1^* despite the decrease in m_w, which is attributed to the increase in the aerodynamic and inertial powers due to the increase in the flapping amplitude.

The hovering efficiency η is mainly dominated by the aerodynamic effect of airfoil, wing response, and inertial power (or wing mass). When Crg2–Crg5 have the respective maximum η, the wing responses and wing masses are almost the same among them (e.g., $\hat{\theta}_{out}$ = 59–60 deg), as shown in Table 4. Thus, the difference in the peak value of η among Crg2–Crg5 is attributed to the aerodynamic effect of the corrugated airfoils; that is, a high amplitude of corrugation is aerodynamically detrimental to the hovering efficiency, as shown in the rigid case. In contrast, Flat and Crg1, which have a spanwise-bending mode, does not attain the preferable feathering angle of 60 deg at $f_1^* > 2$. Although Crg1 attains the feathering angle of 59 deg at $f_1^* = 1.8$, the mode shape stil includes spanwise bending; consequently, the wing mass is heavier than the wings with the chordwise bending (i.e., Crg2–Crg5). At $f_1^* < 2$, the rapid phase shifts in $\psi_{I/O}$ and $\psi_{F/F}$ occur due to resonance. The drastic phase shift in $\psi_{F/F}$ apart from 90 deg reduces η [12,16]. Furthermore, for the wings including spanwise bending in the first mode, the phase shift in $\psi_{I/O}$ is detrimental to the hovering efficiency because of a decrease of $\hat{\phi}_{out}$ and an occurrence of the figure-of-eight stroke deviation. In addition, Flat and Crg1 with the maximum η do not have a trapezoidal waveform but a sinusoidal

waveform of feathering motion, as shown in Figs. 11b, which also reduces η [12,16]. Therefore, the maximum η of Crg1 at $f_1^* < 2$ is smaller than that of Crg2 at $f_1^* > 2$.

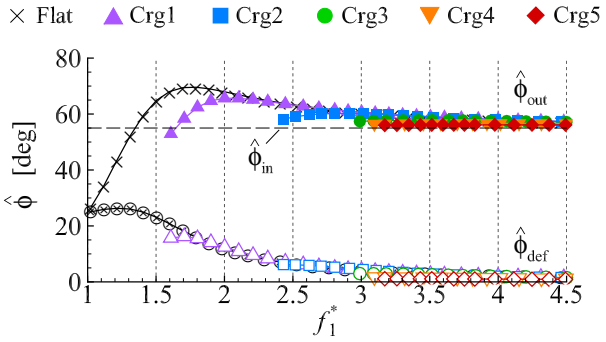

a) Amplitude of the flapping angle

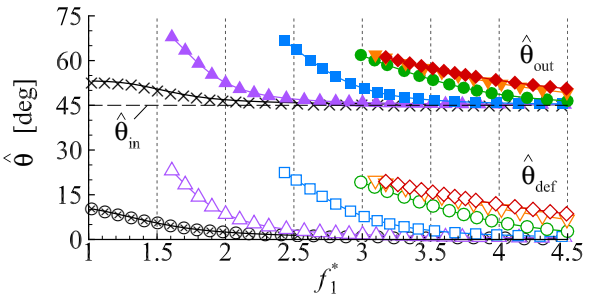

b) Amplitude of the feathering angle

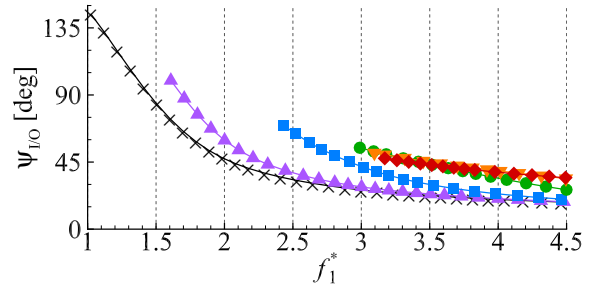

c) Phase lag of the first-mode coordinate between input and output oscillations

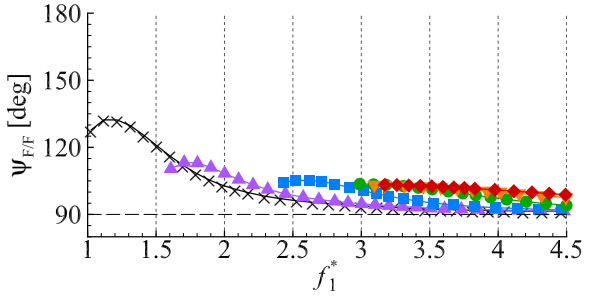

d) Phase lead between the flapping and feathering angles

Fig. 13 Aeroelastic responses with respect to the natural frequency ratio when $\hat{\theta}_{in}$ = 45 deg.

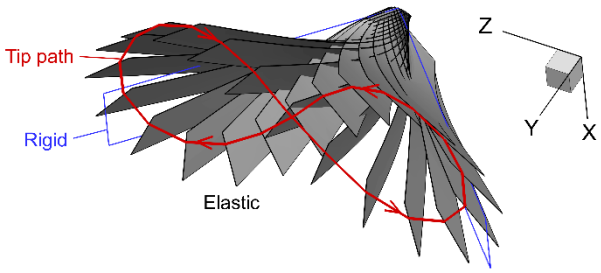

a) Flat at f_1^* = 1.2 when $\hat{\theta}_{in}$ = 45 deg

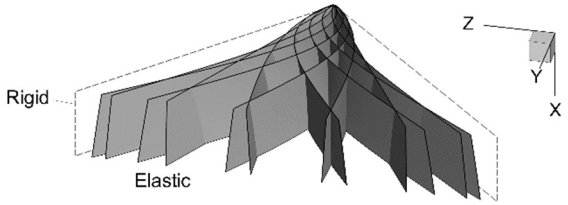

b) Flat at f_1^* = 1.0 when $\hat{\theta}_{in}$ = 0 deg

Fig. 14 Wing motion sequences during a cycle for Flat at f_1^* near resonance.

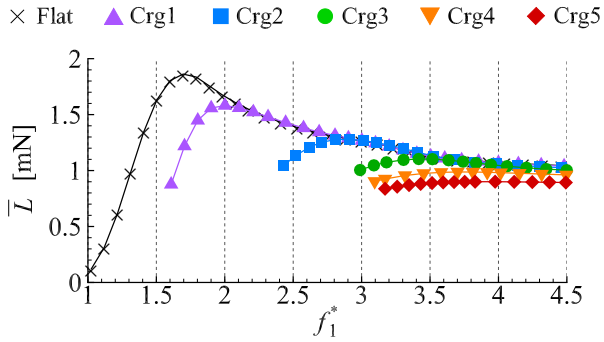

a) Mean lift

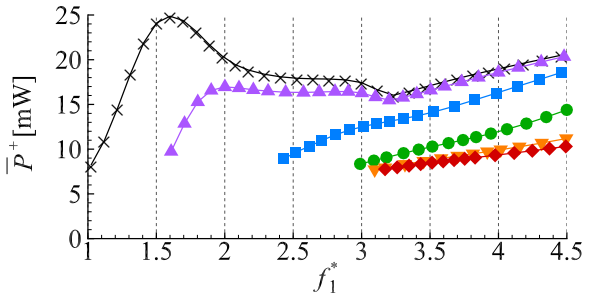

b) Mean total power

Fig. 15 Mean lift and power with respect to the natural frequency ratio when $\hat{\theta}_{in}$ = 45 deg.

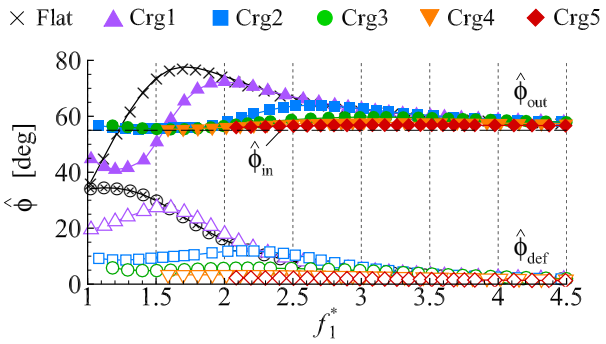

a) Amplitude of the flapping angle

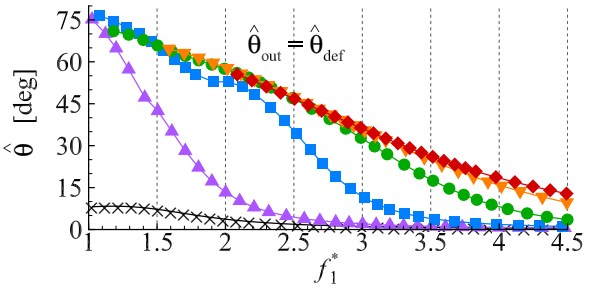

b) Amplitude of the feathering angle

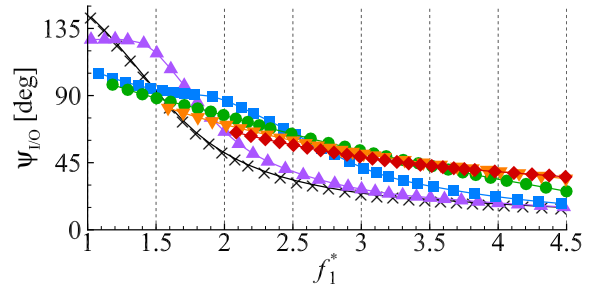

c) Phase lag of the first-mode coordinate between the input and output oscillations

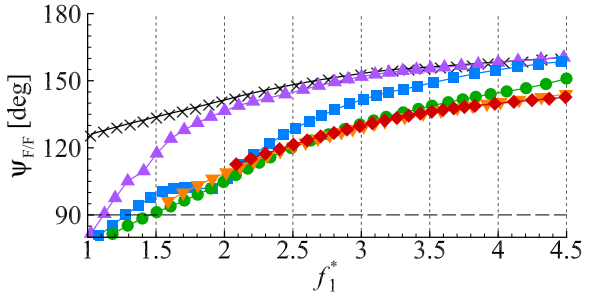

d) Phase lead between the flapping and feathering angles

Fig. 16 Aeroelastic responses with respect to the natural frequency ratio when $\hat{\theta}_{in} = 0$ deg.

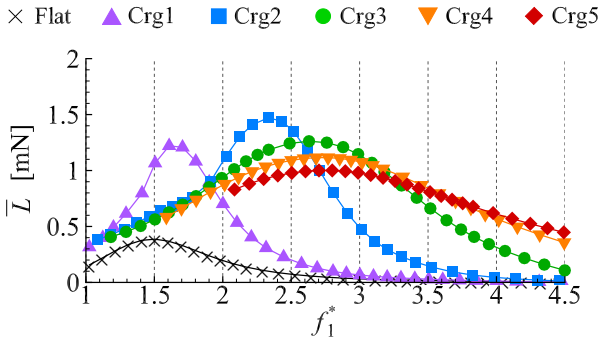

a) Mean lift

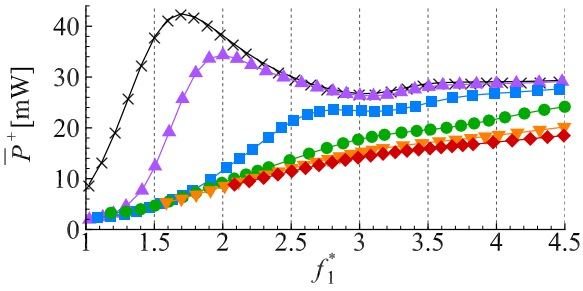

b) Mean total power

Fig. 17 Mean lift and power with respect to the natural frequency ratio when $\hat{\theta}_{in} = 0$ deg.

B. Aeroelastic Responses in Fully Passive Feathering

Figure 16 shows $\hat{\phi}_{\text{out}}$, $\hat{\theta}_{\text{out}}$, $\psi_{\text{I/O}}$, and $\psi_{\text{F/F}}$ with respect to f_1^* when $\hat{\theta}_{\text{in}}$ = 0 deg. Figure 16b indicates that $\hat{\theta}_{\text{out}}$ increases monotonically with decreasing f_1^* for the wings with the chordwise-bending mode (e.g., Crg2–Crg5) due to the decrease in the chordwise flexural rigidity. Figure 16a indicates that Flat has a peak of $\hat{\phi}_{\text{out}}$ at f_1^* = 1.5 although $\hat{\phi}_{\text{def}}$ increases monotonically with decreasing f_1^*. This is attributed to the rapid phase shift in $\psi_{\text{I/O}}$ at $f_1^* < 2$, as shown in Fig. 16c. The increase in $\psi_{\text{I/O}}$ not only reduces $\hat{\phi}_{\text{out}}$ but also produces an inappropriate flapping motion with a phase lag between the wing base and tip, as shown in Fig. 14b. The remarkable difference in the wing response between $\hat{\theta}_{\text{in}}$ = 0 and 45 deg is the relation of $\psi_{\text{I/O}}$ to $\psi_{\text{F/F}}$. When a wing ideally has only a pure chordwise bending without spanwise bending, $\psi_{\text{F/F}}$ = 180 deg − $\psi_{\text{I/O}}$ when $\hat{\theta}_{\text{in}}$ = 0 deg. For the wings in which the chordwise-bending mode is predominant (i.e., Crg3–Crg5), this relation is approximately satisfied; that is, when $\psi_{\text{I/O}}$ increases rapidly from 45 to 90 deg with decreasing f_1^*, $\psi_{\text{F/F}}$ decreases from 135 to 90 deg, which improves the hovering efficiency [12,16]. For the wings including spanwise bending in the first mode (e.g., Flat), the shift in $\psi_{\text{I/O}}$ does not affect the shift in $\psi_{\text{F/F}}$ significantly because it affects both phases of flapping and feathering oscillations at the same time.

The mean lift with respect to f_1^* is shown in Fig. 17a. For Crg2–Crg5, the peaks of lift appear at f_1^* = 2.3–2.8 when $\hat{\theta}_{\text{out}}$ = 42–44 deg; the peak value is larger with a lower a_{w}. In contrast, the peaks of lift for Flat and Crg1 appear at f_1^* = 1.5–1.6, at which $\hat{\phi}_{\text{out}}$ has almost the maximum value. The peak values of lift for Flat and Crg1 are smaller than those of Crg2 because $\hat{\theta}_{\text{out}}$ is as small as 6 deg for Flat and 35 deg for Crg1. The mean total power with respect to f_1^* is shown in Fig. 17b. The total power of each wing model tends to decrease with decreasing f_1^* because of the decrease in the wing mass and the increase in the feathering amplitude. Similar to the case with $\hat{\theta}_{\text{in}}$ = 45 deg, the difference in total power among Flat–Crg5 is mainly attributed to that in wing mass; that is, the wings with the chordwise-bending mode have a lighter weight and reduce the inertial power. In contrast, the wings with the spanwise-bending mode (e.g., Flat and Crg1) need larger total power because of the larger flapping amplitude and the heavier wing mass than the others.

As shown in Fig. 10b, the peaks of η appear at f_1^* = 2.1–2.3 for Crg2–Crg5. Among the four wings, the wing responses and wing masses are almost the same (e.g., $\hat{\theta}_{\text{out}}$ = 51–54 deg), as shown in Table 4. Thus, the difference in the peak value of η among Crg2–Crg5 is attributed only to the aerodynamic effect of the corrugated airfoils. In contrast, on the peaks of Crg1 and Crg2 at $f_1^* < 2$, $\hat{\theta}_{\text{out}}$ = 65–70 deg, which is larger than the feathering angle of 51–54 deg for Crg3–Crg5 with peak η. Furthermore, the drastic phase shift in $\psi_{\text{I/O}}$ at $f_1^* < 2$ causes an inappropriate flapping motion, as shown in Fig. 14b. Therefore, Crg2 at f_1^* = 2.1 has the maximum η of all the wings.

C. Effects of High-Order Modes

In this section, the effects of high-order modes on the aeroelastic characteristics of the corrugated flapping wings are discussed. Figure 18 shows the intensity (root mean square) of each modal coordinate with respect to f_1^*. The intensity in the third mode is not shown on the graph because it is much smaller than the others. When $\hat{\theta}_{\text{in}}$ = 45 deg, the effect of the second mode is much lower than that of the first mode; therefore, the previous discussion focusing on the behavior of the first mode is valid. When $\hat{\theta}_{\text{in}}$ = 0 deg, the intensity of the second mode increases at $f_1^* < 2.5$. The representative second mode shapes for Flat–Crg5 at f_1^* = 2.0 are shown in Fig. 19. All the second modes have similar spanwise torsion, and no remarkable mode conversion with respect to f_1^* occurs unlike that for the first modes. To evaluate the effect of the second mode on the aeroelastic characteristics, we conducted an identical aeroelastic simulation using only the first mode and neglecting the second and third modes. The hovering efficiency calculated with only the single mode is shown in Fig. 20, in addition to the results calculated with the three modes shown in Fig. 10. When $\hat{\theta}_{\text{in}}$ = 45 deg, the results with the single mode show good agreement with those with the three modes. In contrast, when $\hat{\theta}_{\text{in}}$ = 0 deg, there is a large discrepancy of η at $1.3 < f_1^* < 2.5$ due to the excitation of the second mode, which indicates that the dips of η at $1.3 < f_1^* < 2.2$ for Crg2 and Crg3 in the calculation with the three modes are mainly attributed to the excitation of the second modes. To elaborate the wing motions when the dip of η appears, the time histories of the flapping and feathering motions for Crg2 with the single and with the three modes are shown in Fig. 21. In comparison with Figs 21a and 21b, it can be seen that the feathering motions calculated with the three modes do not have a trapezoidal waveform but have a twin-peak waveform in each up- and downstroke at $1.3 < f_1^* < 2.2$. This result indicates that the second mode extremely enhances the third-harmonic oscillation of the feathering motion in $1.3 < f_1^* < 2.2$, which causes a

reduction in the hovering efficiency. Further study is necessary to clarify the effects of high-order modes and high harmonics on the aeroelastic characteristics of a flapping wing. However, as can be seen from Fig. 20, the maximum η appears at almost the same f_1^* (i.e., the same structural design) between the calculations with the single and three modes; f_1^* = 1.0 and 1.0 for Flat, 1.3 and 1.2 for Crg1, 1.9 and 2.1 for Crg2, 2.0 and 2.3 for Crg3, 2.1 and 2.2 for Crg4, and 2.2 and 2.3 for Crg5 in the calculations with the single and three modes, respectively. Therefore, the previous discussion focusing on the vibrational behavior of the first mode is still valid for explaining the fundamental aeroelastic characteristics of the corrugated flapping wings.

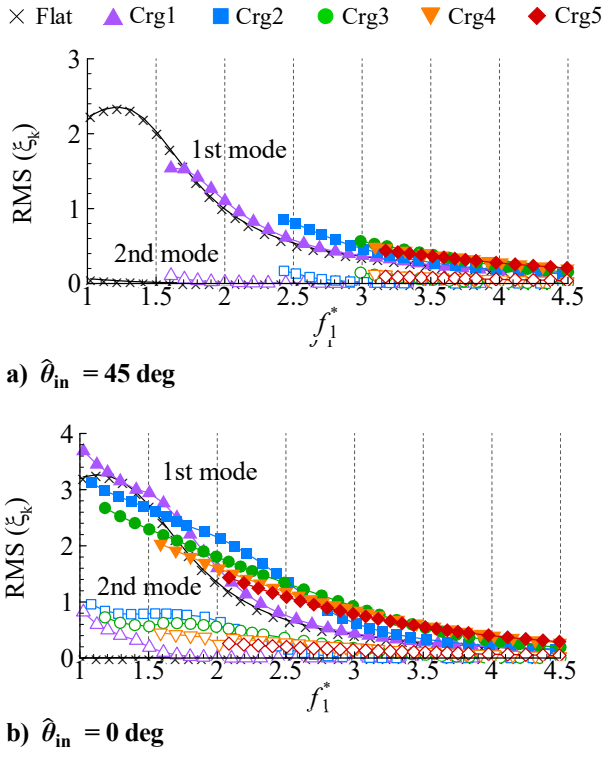

Fig. 18 Root mean square of the modal coordinates with respect to the natural frequency ratio.

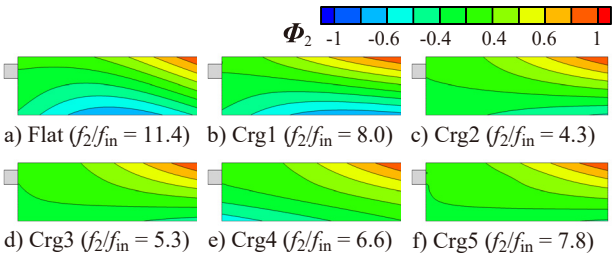

Fig. 19 Second modes (torsional modes) at f_1^* = 2.0.

D. Optimal Structure of a Corrugated Flapping Wing

In this study, the optimal wing was Crg2 at f_1^* = 2.6 when $\hat{\theta}_{in}$ = 45 deg and Crg2–Crg3 at f_1^* = 2.1–2.3 when $\hat{\theta}_{in}$ = 0 deg, both of which have chordwise bending in the first mode. For the wings with the chordwise-bending mode, the maximum η appears when the feathering motion has an appropriate amplitude and phase, which is dominated by an appropriate modal stiffness (i.e., f_1^*). The wings including spanwise bending in the first mode are not preferable for obtaining a high efficiency because they have a heavier wing mass than the wings with the chordwise-bending mode, as shown in Fig. 8. For a corrugated wing, an increase in a_w or a decrease of h yields chordwise bending in the first mode. However, the airfoil with a higher a_w reduces the hovering efficiency due to the negative aerodynamic effect of corrugation; thus, a corrugated airfoil with a lower a_w is preferable in terms of aerodynamics. To attain the chordwise-bending mode with a lower a_w, a much thinner h is required, which results in a decrease in f_1^*. Therefore, it is difficult for the wings with a lower a_w to attain both the chordwise-bending mode and the appropriate modal stiffness (i.e., f_1^*). Furthermore, when f_1^* decreases less than about two (i.e., $f_{in}/f_1 > 0.5$), a drastic phase shift in $\psi_{I/O}$ occurs because the resonance is approached, which is detrimental to the hovering efficiency, especially for the wings with the spanwise-bending mode because of the occurrence of an inappropriate flapping motion (i.e., a phase lag between the wing base and tip and/or a large stroke deviation). In addition, at $f_1^* < 2$, the high-order modes induce detrimental high-harmonic oscillation to the wing response, which also decreases η. Therefore, the optimal wing satisfies two conditions: (1) the amplitude of corrugation is as low as possible in terms of aerodynamics, and (2) the chordwise-bending mode attains as

high a f_1^* as possible without the influences of drastic phase shift due to resonance and the excitation of high-order modes. The amplitude of corrugation for the optimal wings, or Crg2 and Crg3, is 1.7–2.6% c, which is close to 1.4–3.3% c of the measured data of several insect wings [33]. The wing mass ratio for the optimal wings (m_w^* = 0.7–1.5) is also close to that for the baseline model (m_w^* = 1.9). These agreements between the optimal wings and insect wings indicate that insects utilize corrugation to attain both preferable aeroelastic deformation and wing-weight reduction. Furthermore, the optimal f_1^* of 2.1–2.6 (i.e., f_{in}/f_1 = 0.38–0.48 as a conventional expression) is close to those shown in previous studies (f_{in}/f_1 = 0.4 [22], 0.5–0.6 [31], and 0.3–0.35 [54]).

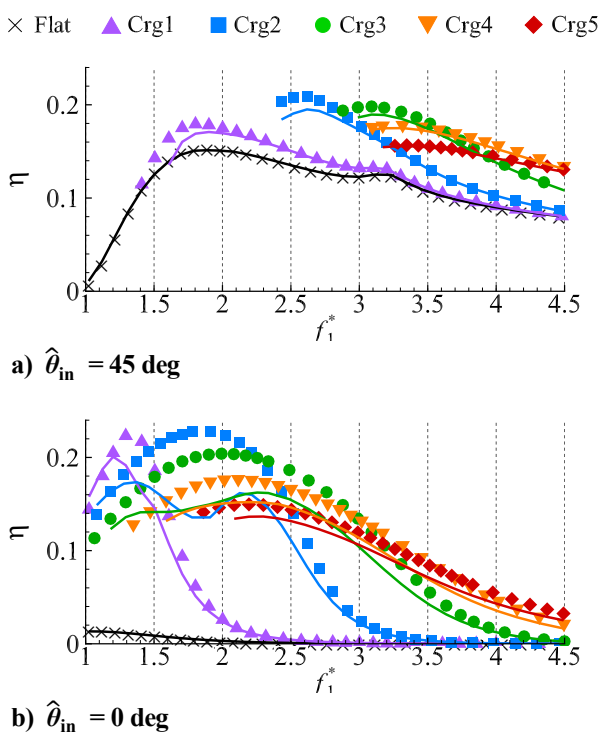

a) $\hat{\theta}_{in}$ = 45 deg

b) $\hat{\theta}_{in}$ = 0 deg

Fig. 20 Hovering efficiency with respect to the natural frequency ratio calculated using only the single first mode (markers) and the three modes (solid lines).

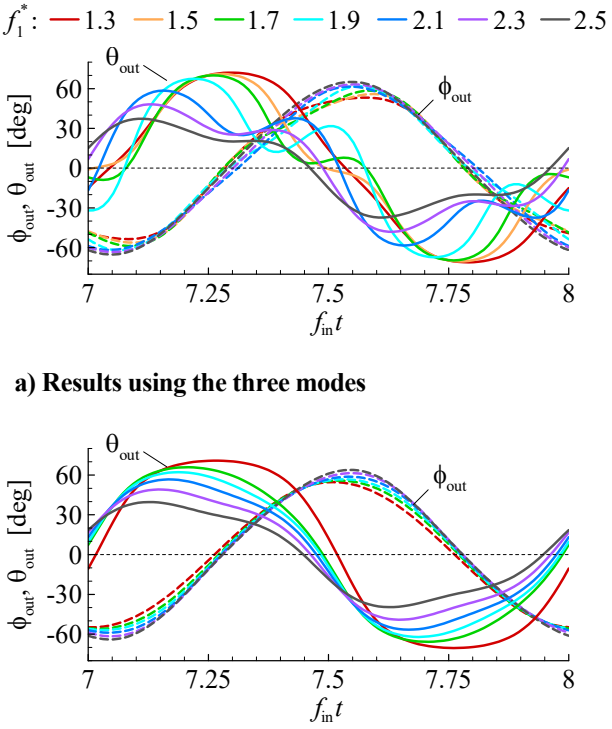

a) Results using the three modes

b) Results using the single first mode

Fig. 21 Time histories of the flapping and feathering motions during a cycle at r_{ref} for Crg2 at f_1^* = 1.3 to 2.5 when $\hat{\theta}_{in}$ = 0 deg.

The structural parameters of the optimal wings (f_1^* = 2.1–2.6 are m_w^* = 0.7–1.5) are slightly smaller than those of the baseline model (f_1^* = 3.6 and m_w^* = 1.9), which indicates that the plate thickness of the optimal wings is thinner than that of the baseline model. This disagreement indicates that insect wings are designed conservatively in comparison with the optimal wings. In this study, the strength of the wing structure was not considered despite the large deformation occurring in the optimal wings. If the strength and fatigue of the wing material are considered, a more conservative design with a larger thickness (i.e., a larger f_1^*) could be obtained in the numerical result. The optimal wing structure can be obtained not only by corrugation but also by an anisotropic material. If a highly anisotropic material is employed, even a flat wing could achieve such an optimal structure with a light weight. However, according to previous studies [35,48], the material properties of veins and membranes for insect wings are comparable to each other. Therefore, the structural anisotropy of insect wings is provided by corrugation and veins rather than anisotropic material. If the wing was reinforced by only veins without corrugation, the veins as thick as the corrugation would be required when a similar material is used, which would lead to a similar conclusion to the corrugated wings shown in this study. The results shown in this study indicate that the corrugation is useful for an elastic flapping wing to enhance the aerodynamic performance even without veins. Thus, if the corrugation was combined with veins, higher aerodynamic

performance would be expected. Actually, the veins of insect wings are usually placed at the vertices of corrugation [33], which reinforces the flexural rigidity and enhance the aerodynamic performance with a decrease of the required amplitude of corrugation. Although the corrugation in this study is implemented homogeneously and globally on the wing surface, the designs of insect wings are more complicated. A local arrangement of veins and corrugation can provide a more preferable wing deformation. In contrast to the wing model in this study, the elastic flapping wings with a local reinforcement generate positive camber deformation in both the up- and downstrokes, which improves the aerodynamic performance [23, 30, 32]. In future work, it is necessary to investigate an optimal combination and arrangement of corrugation and veins for an elastic flapping wing in both hovering and forward flights.

VI. Conclusions

In this study, the authors numerically investigated the fundamental aeroelastic effects of corrugation of an insect-sized flapping wing in hovering flight. A simple, reasonable structural model for an insect-sized corrugated flapping wing was constructed as a baseline, which was based on the material properties of bumblebee wings. The aeroelastic characteristics were calculated for the corrugated flapping wings by changing the thickness and amplitude of corrugation around the baseline model, which modulated the natural frequencies and mode shapes of the wing. The numerical results indicate that the optimal wing to maximize the hovering efficiency has an amplitude of corrugation of 1.7–2.6% chord length, a natural frequency that is 2.1–2.6 times as large as the input frequency, and a wing mass ratio of 0.7–1.5. These structural parameters are close to but slightly smaller than the values of the baseline model. Therefore, the results indicate that the corrugation of insect flapping wings is aeroelastically effective in providing both an appropriate passive deformation and a lightweight wing. The optimal flapping wing has chordwise bending in the first mode, which is attained by a reduction in the thickness or an increase in the amplitude of corrugation. However, a higher amplitude of corrugation is detrimental to the hovering efficiency. In contrast, a reduction in the thickness results in a decrease in the natural frequency, which causes a very large torsion. Furthermore, a natural frequency less than two times as large as the input frequency causes a rapid phase shift between the output and input oscillation due to resonance and induces detrimental high-harmonic oscillation due to the high-order modes, significantly reducing the hovering efficiency. Therefore, the optimal wing with the chordwise-bending mode is attained by trade-off between the amplitude of corrugation, which must be as low as possible, and the natural frequency, which should be sufficiently high for the effects of phase shift and high-order modes to be neglected. The results indicate that the corrugation is useful for an elastic flapping wing to enhance the aerodynamic performance even with an isotropic material. With local arrangement and combination of veins and corrugation like insect wings, the elastic flapping wings would be expected to improve the aerodynamic performance even without a highly anisotropic material.

Appendix: Comparison between 2-D and 3-D models

To validate the 2-D shell model for the wing structure with corrugation, we compared the first natural frequencies between the 2-D shell and 3-D solid models. Three-dimensional 20-node solid elements (SOLID186) were arranged 225 in the spanwise, 85 in the chordwise, and 2 in the thickwise direction (Consequently, 38,250 elements and 212,183 nodes). The error of the first natural frequencies between the 2-D shell and 3-D solid models are shown in Table A1. The error increases as a_w increases and $2a_w/h$ decreases. The maximum error is 7.9% at $f_1^* = 4.5$ for Crg2. In the case with a maximum η, the frequency error is 2.3% or less when $\hat{\theta}_{in} = 0$ deg, 3.3% or less when $\hat{\theta}_{in} = 45$ deg. This result indicates that the modal analysis with the 2-D shell model is valid in the parameter range of this study.

Table A1 Error of the first natural frequencies between 2-D shell and 3-D solid models

Wing	$(f_1 - f_{1,3D})/f_{1,3D}$		
	Max η in $\hat{\theta}_{in} = 0$ deg	Max η in $\hat{\theta}_{in} =$ 45 deg	$f_1^* = 4.5$
Flat	0.2% ($f_1^* = 1.0$)	0.2% ($f_1^* = 1.9$)	0.2%
Crg1	1.7% ($f_1^* = 1.2$)	2.6% ($f_1^* = 1.9$)	4.0%
Crg2	2.0% ($f_1^* = 2.1$)	2.8% ($f_1^* = 2.6$)	7.9%
Crg3	1.5% ($f_1^* = 2.3$)	2.5% ($f_1^* = 3.1$)	5.9%
Crg4	1.2% ($f_1^* = 2.2$)	2.2% ($f_1^* = 3.3$)	3.7%
Crg5	1.0% ($f_1^* = 2.3$)	1.7% ($f_1^* = 3.3$)	3.0%

Acknowledgements

This work was supported in part by Japan Society for the Promotion of Science Grants-in-Aid for Scientific Research (grant numbers JP15K18284 and JP19K04838). The authors would like to thank Yasuhiro Takaku and Masahiko Hirota for providing the material properties of bumblebee wings. The computation was performed using the computer resources offered under the category of General Projects by Research Institute for Information Technology, Kyushu University.

References

[1] Keennon, M., Klingebiel, K., Won, H., and Andriukov, A., "Development of the Nano Hummingbird: A Tailless Flapping Wing Micro Air Vehicle," *50th AIAA Aerospace Sciences Meeting including the New Horizons Forum and Aerospace Exposition*, January 2012, AIAA 2012-588.
doi: 10.2514/6.2012-588

[2] Roshanbin, A., Altartouri, H., Karásek, M., Preumont, A., "COLIBRI: A Hovering Flapping Twin-Wing Robot," *International Journal of Micro Air Vehicles*, Vol. 9, No. 4, 2017, pp. 270–282.
doi: 10.1177/1756829317695563

[3] Karásek, M., Muijres, F. T., De Wagter, C., Remes, B. D. W., de Croon, G. C. H. E., "A Tailless Aerial Robotic Flapper Reveals That Flies Use Torque Coupling in Rapid Banked Turns," *Science*, Vol. 361, Issue 6407, 2018, pp. 1089–1094.
doi: 10.1126/science.aat0350

[4] Phan, H. V., Aurecianus, S., Kang, T., and Park, H. C., "KUBeetle-S: An Insect-like, Tailless, Hover-Capable Robot that can Fly with a Low-Torque Control Mechanism," *International Journal of Micro Air Vehicles*, Vol. 11, January 2019, pp. 1–10.
doi: 10.1177/1756829319861371

[5] Nagai, H., Nakamura, K, Fujita, K., Tanaka, I., Nagasaki, S., Kinjo, Y., Kuwazono, S., and Murozono, M., "Development of Tailless Two-Winged Flapping Drone with Gravity Center Position Control," *Sensors and Materials*, Vol. 33, No. 3, 2021, pp. 859–872.
doi: 10.18494/SAM.2021.3222

[6] Hoang, V., P., and Hoon, C., P., "Insect-Inspired, Tailless, Hover-Capable Flapping-Wing Robots: Recent Progress, Challenges, and Future Directions," *Progress in Aerospace Sciences*, Vol. 111, November 2019, Paper 100573.
doi: 10.1016/j.paerosci.2019.100573

[7] Ellington, C. P., Van den Berg, C., Willmott, A. P., and Thomas, A. L. R., "Leading-Edge Vortices in Insect Flight," *Nature*, Vol. 384, Dec. 1996, pp. 626–630.
doi: 10.1038/384626a0

[8] Dickinson, M. H., Lehmann, F. -O., and Sane, S. P., "Wing Rotation and the Aerodynamic Basis of Insect Flight," *Science*, Vol. 18, Jun. 1999, pp. 1954–1960.
doi: 10.1126/science.284.5422.1954

[9] Isogai, K., Fujishiro, S., Saitoh, T., Yamamoto, M., Yamasaki, M., and Matsubara, M., "Unsteady Three-Dimensional Viscous Flow Simulation of a Dragonfly Hovering," *AIAA journal*, Vol. 42, No. 10, 2004, pp. 2053–2059.

doi: 10.2514/1.6274
[10] Yamamoto, M., and Isogai, K., "Measurement of Unsteady Fluid Dynamic Forces for a Mechanical Dragonfly Model," *AIAA Journal*, Vol. 43, No. 12, 2005, pp. 2475–2480.
doi: 10.2514/1.15899
[11] Nagai, H., Isogai, K., Fujimoto, T., and Hayase, T., "Experimental and Numerical Study of Forward Flight Aerodynamics of Insect Flapping Wing," *AIAA Journal*, Vol. 47, No. 3, 2009, pp. 730–742.
doi: 10.2514/1.39462
[12] Nagai, H., and Isogai, K., "Effects of Flapping Wing Kinematics on Hovering and Forward Flight Aerodynamics," *AIAA Journal*, Vol. 49, No. 8, 2011, pp. 1750–1762.
doi: 10.2514/1.J050968
[13] Sun, M. an Tang, J., "Lift and Power Requirements of Hovering Flight in Drosophila Virilis," *Journal of Experimental Biology*, Vol. 205, No. 16, 2002, pp. 2413–2427.
doi: 10.1242/jeb.205.16.2413
[14] Lehmann, F.-O., "Wing-Wake Interaction reduces power consumption in Insect Tandem Wings," *Experiments in Fluids*, Vol. 46, May 2009, pp. 765–775.
doi: 10.1007/s00348-008-0595-0
[15] Nagai, H., Fujita, K., and Murozono, M., "Experimental Study on Forewing-Hindwing Phasing in Hovering and Forward Flapping Flight," *AIAA Journal*, Vol. 57, No. 9, 2019, pp. 3779–3790.
doi: 10.2514/1.J058335
[16] Sane, S. P. and Dickinson, M. H., "The Control of Flight Force by a Flapping Wing: Lift and Drag Production," *Journal of Experimental Biology*, Vol. 204, No. 15, 2001, pp. 2607–2626.
doi: 10.1242/jeb.204.15.2607
[17] Walker, S. M., Thomas, A. L. R., and Taylor, G. K., "Deformable Wing Kinematics in the Desert Locust: How and Why Do Camber, Twist and Topography Vary Through the Stroke?," *Journal of the Royal Society Interface*, Vol. 6, Issue 38, 2009, pp. 735–747.
doi: 10.1098/rsif.2008.0435
[18] Walker, S. M., Thomas, A. L. R., and Taylor, G. K., "Deformable Wing Kinematics in Free-Flying Hoverflies," *Journal of the Royal Society Interface*, Vol. 7, Issue 42, 2010, pp. 131-142.
doi: 10.1098/rsif.2009.0120
[19] Young, J., Walker, S. M., Bomphrey, R. J., Taylor, G. K., and Thomas, A. L. R., "Details of Insect Wing Design and Deformation Enhance Aerodynamic Function and Flight Efficiency," *Science*, Vol. 325, No. 5947, 2009, pp. 1549–1552.
doi: 10.1126/science.1175928
[20] Du, G. and Sun, M., "Effects of Wing Deformation on Aerodynamic Forces in Hovering Hoverflies," *Journal of Experimental Biology*, Vol. 213, No. 13, 2010, pp. 2273–2283.
doi: 10.1242/jeb.040295
[21] Ishihara, D., Horie, T. and Denda, M., "A Two-Dimensional Computational Study on the Fluid–Structure Interaction Cause of Wing Pitch Changes in Dipteran Flapping Flight", *Journal of Experimental Biology*, Vol. 212, No. 1, 2009, pp. 1–10.
doi: 10.1242/jeb.020404
[22] Kang, C., Aono, H., Cesnik, C. E. S., Shyy, W., "Effects of Flexibility on the Aerodynamic Performance of Flapping Wings," *Journal of Fluid Mechanics*, Vol. 689, November 2011, pp. 32–74.
doi: 10.1017/jfm.2011.428
[23] Nakata, T. and Liu, H., "A Fluid–Structure Interaction Model of Insect Flight with Flexible Wings", *Journal of Computational Physics*, Vol. 231, No. 4, 2012, pp. 1822–1847.
doi: 10.1016/j.jcp.2011.11.005
[24] Kang, C, Shyy, W. "Scaling Law and Enhancement of Lift Generation of an Insect-Size Hovering Flexible Wing," *Journal of the Royal Society Interface*, Vol. 10, Issue 85, 2013, Paper 20130361.
doi: 10.1098/rsif.2013.0361
[25] Gogulapati, A., Friedmann, P. P., Kheng, E., and Shyy, W., "Approximate Aeroelastic Modeling of Flapping Wings in Hover", *AIAA Journal*, Vol. 51, No. 3, Mar. 2013, pp. 567–583.
doi: 10.2514/1.J051801

[26] Tobing, S., Young, J., Lai, J. C. S., "Effects of Wing Flexibility on Bumblebee Propulsion," *Journal of Fluids and Structures*, Vol. 68, January 2017, pp. 141–157.
doi: 10.1016/j.jfluidstructs.2016.10.005

[27] Kolomenskiy, D., Ravi, S., Xu, R., Ueyama, K., Jakobi, T., Engels, T., Nakata, T., Sesterhenn, J., Schneider, K., Onishi, R., Liu, H., "The Dynamics of Passive Feathering Rotation in Hovering Flight of Bumblebees," *Journal of Fluids and Structures*, Vol. 91, November 2019, Paper 102628.
doi: 10.1016/j.jfluidstructs.2019.03.021

[28] Ishihara, D., Yamashita, Y., Horie, T., Yoshida, S., and Niho., T., "Passive Maintenance of High Angle of Attack and its Lift Generation during Flapping Translation in Crane Fly Wing," *Journal of Experimental Biology*, Vol. 212, No. 23, 2009, pp. 3882–3891.
doi: 10.1242/jeb.030684

[29] Wu, P. and Ifju, P., "Flapping Wing Structural Deformation and Thrust Correlation Study with Flexible Membrane Wings", *AIAA Journal*, Vol. 48, No. 9, 2010, pp. 2111–2122.
doi: 10.2514/1.J050310

[30] Truong, T. V., Nguyen, Q. –V., and Lee, H. P., "Bio-Inspired Flexible Flapping Wings with Elastic Deformation", *Aerospace*, Vol. 4, No. 3, 2017, Paper 37.
doi: 10.3390/aerospace4030037

[31] Ramananarivo, S., Godoy-Diana, R., and Thiria, B., "Rather than Resonance, Flapping Wing Flyers may Play on Aerodynamics to Improve Performance," *Proceedings of the National Academy of Sciences of the United States of America*, Vol. 108, No. 15, 2011, pp. 5964–5969.
doi: 10.1073/pnas.1017910108

[32] Addo-Akoto, R., Han, J. S., Han, J. H., "Roles of Wing Flexibility and Kinematics in Flapping Wing Aerodynamics," *Journal of Fluids and Structures*, Vol. 104, July 2021, Paper 103317.
doi: 10.1016/j.jfluidstructs.2021.103317

[33] Rees, C., "Form and Function in Corrugated Insect Wings," *Nature*, Vol. 256, July 1975, pp. 200–203.
doi: 10.1038/256200a0

[34] Combes, S. A. and Daniel, T. L., "Flexural Stiffness in Insect Wings I. Scaling and the Influence of Wing Venation," *Journal of Experimental Biology*, Vol. 206, No. 17, 2003, pp. 2979–2987.
doi: 10.1242/jeb.00523

[35] Combes, S. A., "Materials, Structure, and Dynamics of Insect Wings as Bioinspiration for MAVs," *Encyclopedia of Aerospace Engineering*, 2010, pp. 1–10.
doi: 10.1002/9780470686652.eae404

[36] Nagai, H., Isogai, K., Uda, N., and Ono, K., "Investigation on Airfoil for an Insect-Sized Flapping Wing," *Proceedings of 29th International Congress of the Aeronautical Sciences*, 2014, Paper ICAS 2014-4.3.3.
doi: N/A

[37] Vargas, A., Mittal, R., and Dong, H. "A Computational Study of the Aerodynamic Performance of a Dragonfly Wing Section in Gliding Flight," *Bioinspiration and Biomimetics*, Vol. 3, No. 2, 2008, Paper 026004.
doi: 10.1088/1748-3182/3/2/026004

[38] Levy, D. –E. and Seifert, A., "Parameter Study of Simplified Dragonfly Airfoil Geometry at Reynolds Number of 6000," *Journal of Theoretical Biology*, Vol. 266, No. 4, 2010, pp. 691–702.
doi: 10.1016/j.jtbi.2010.07.016

[39] Hu, H. and Tamai, M., "Bioinspired Corrugated Airfoil at Low Reynolds Numbers," *Journal of Aircraft*, Vol. 45, No. 6, 2008, pp. 2068–2077
doi: 10.2514/1.37173

[40] Obata, A. and Sinohara, S., "Flow Visualization Study of the Aerodynamics of Modeled Dragonfly Wings," *AIAA journal*, Vol. 47, No. 12, 2009, pp. 3043–3048.
doi: 10.2514/1.43836

[41] Meng, X. G., Xu, L., and Sun, M., "Aerodynamic Effects of Corrugation in Flapping Insect Wings in Hovering Flight," *Journal of Experimental Biology*, Vol. 214, No. 3, 2011, pp. 432–444.
doi: 10.1242/jeb.046375

[42] Meng, X. and Sun, M., "Aerodynamic Effects of Corrugation in Flapping Insect Wings in Forward Flight," *Journal of*

Bionic Engineering, Vol. 8, No. 2, 2011, pp. 140–150.
doi: 10.1016/S1672-6529(11)60015-2

[43] Du, G. and Sun, M., "Aerodynamic Effects of Corrugation and Deformation in Flapping Wings of Hovering Hoverflies," *Journal of Theoretical Biology*, Vol. 300, May 2012, pp. 19–28.
doi: 10.1016/j.jtbi.2012.01.010

[44] Au, L. T., K., Phan, H. V., Park, S. H., and Park, H. C., "Effect of Corrugation on the Aerodynamic Performance of Three-Dimensional Flapping Wings," *Aerospace Science and Technology*, Vol. 105, Oct. 2020, Paper 106041.
doi: 10.1016/j.ast.2020.106041

[45] Dao, T. T., Loan Au, T. K., Park, S. H., and Park, H. C., "Effect of Wing Corrugation on the Aerodynamic Efficiency of Two-Dimensional Flapping Wings," *Applied Science*, Vol. 10, No. 20, 2020, Paper 7375.
doi: 10.3390/app10207375

[46] Kesel, A. B., Philippi, U., and Nachtigall, W., "Biomechanical Aspects of the Insect Wing: An Analysis using the Finite Element Method," *Computers in Biology and Medicine*, Vol. 28, No. 4, 1998, pp. 423–437.
doi: 10.1016/S0010-4825(98)00018-3

[47] Dudley, R. and Ellington, C. P., "Mechanical of Forward Flight in Bumblebees I. Kinematics and Morphology," *Journal of Experimental Biology*, Vol. 148, No. 1, 1990, pp. 19–52.
doi: 10.1242/jeb.148.1.19

[48] Takaku, Y., "Tensile Testing for Microsize Materials in Tiny Loads," *IIC Review*, No.42, 2009, pp.27–32, IHI Inspection and Instrumentation Co., Ltd. (in Japanese).
doi: N/A

[49] Wainwright, S., A., Biggs, W., D., Currey, J., D., and Gosline, J., M., "Mechanical Design in Organisms," London, Edward Arnold (1976).
doi: 10.1515/9780691218090

[50] Pulliam, T. H. and Steger, J. L., "Implicit Finite-Difference Simulations of Three-Dimensional Compressible Flow," *AIAA Journal*, Vol, 18, No. 2, 1980, pp. 159–167.
doi: 10.2514/3.50745

[51] Yee, H. C. and Harten, A., "Implicit TVD Scheme for Hyperbolic Conservation Laws in Curvilinear Coordinates," *AIAA Journal*, Vol. 25, No. 2, 1987, pp. 266–274.
doi: 10.2514/3.9617

[52] Thomas, P. D. and Lombard, C. K., "Geometric Conservation Law and Its Application to Flow Computations on Moving Grids," *AIAA Journal*, Vol. 17, No. 10, 1979, pp. 1030–1037.
doi: 10.2514/3.61273

[53] Nagai, H., Isogai, K., Murozono, M., and Fujishiro, T., "Investigation on Structural and Aerodynamic Characteristics of Resonant Type Elastic Flapping Wing," *Proceedings of 28th International Congress of the Aeronautical Sciences*, 2012, Paper ICAS 2012-9.5.3.
doi: N/A

[54] Dai, H., Luo, H., and Doyle, J. F., "Dynamic Pitching of an Elastic Rectangular Wing in Hovering Motion," *Journal of Fluid Mechanics*, Vol. 693, January 2012, pp. 473–499.
doi: 10.1017/jfm.2011.543